National and Kapodistrian University of Athens
School of Sciences
Faculty of Geology and Geoenvironment
Oceanography and Management of Marine Environment
Specialization: Geological Oceanography

A Dissertation For The Degree Of MASTER OF SCIENCE In
Oceanography and Management of Marine Environment

Paleoceanographic evolution of the North Aegean Sea during the last 4.0 ka

Maria Fatourou
213007

Supervisor
Prof. Maria Triantaphyllou

Assessment Committee
As. Prof. Margarita Dimiza
Dr. Alexandra Gogou

Athens, 2017

Acknowledgements

This thesis would not have been possible without the help of so many people in many ways.

I would like to thank my supervisor Prof. Maria Triantaphyllou for her continuous support and patience. I would also like to express my deepest gratitude to Dr. Margarita Dimiza who was always willing to help through her comments and criticism. I would like to thank Dr. Alexandra Gogou who provided me the opportunity to have access to the laboratory and research facilities at the HCMR along with Dr. Constantine Parinos.
Furthermore, I thank Dr. Elena Xoplaki for giving me the opportunity to learn many new things during my last semester of MSc studies in the framework of Erasmus+ student mobility stay at the Justus Liebig University of Giessen. I would also like to thank Prof. Juerg Luterbacher for his useful critiques. Moreover from the part of my 'Giessen experience' I want to thank all the members of the Klima group who provided an excellent atmosphere, especially Dr. Stella Dafka and Dr. Martin Ivanov who helped me a lot, despite their busy schedules.
In addition, I want to thank my friend Dr. Dafni Sifnioti for her endless support, my friend Francesca Paraskos for her guidance and help throughout our collaboration at the HCMR, my friend Dr. Mairy Athanasiou for her help and advice.

Lastly, I would like to dedicate this dissertation, to my family for believing in me and supporting me throughout the struggle with my MSc degree and university years.

Cover picture: Skyros basin-sunset during the Kripis project oceanographic cruise, photo: M.F

Table of Contents

Abstract

During the last decades, a variety of scientific studies have shown and supported that marine sediments preserve a wealth of information for the reconstruction of ocean and climate history in the form of their microfossil assemblage, organic matter, elemental and isotopic composition of fossils. Nowadays, it is possible to combine data from marine sediment analysis and climatic models to provide even more information about the paleoceanographic and paleoclimatic conditions of an area of interest.

This research focuses on reconstructing past climatic changes of the North Aegean, due to its unique physical and geographic characteristics with the use of climate models and marine fossil analysis.

The high resolution marine record established for the past 1500 years in the North Aegean Sea, Greece (multicore M2, Athos basin, 1018 m depth) was used to provide palaeoclimatic data from the fluctuations of the isotopic signal of the planktonic foraminifer *Globigerinoides ruber*. In addition, changes in dissolved oxygen concentrations in the pore and bottom waters at the same site, were obtained by relative abundance of the benthic foraminiferal low oxygen indicators and the subsequent calculation of Low Oxygen -index. Also, the multicore M3, retrieved from Skyros basin, was used to provide alkenone Sea Surface Temperatures for 1600 to 600 BC.

The climatic model data were provided from the simulations of the Coupled Model Intercomparison Project (CMIP5) for the last 2000 years. In particular, the MPI-ESM-P-p2k, the MPI-ESM-P r1 and the CCSM4 r1 simulations for this specific area were analyzed on annual and seasonal resolution. Via the analysis, short-term changes in temperature and humidity were examined and correlated with the d $^{18}O_{G.ruber}$ isotopic signal in relation to alkenone Sea Surface Temperature record, the upper water column Stratification index and the bottom waters Low-Oxygen index. Through this multi proxy methodology the climatic conditions of the Roman Warm Period, the Dark Ages, the Late Antique Little Ice Age, the Medieval Climate Anomaly and the Little Ice Age were sufficiently coupled with the paleoceanographic-paleoclimatic reconstruction for the North Aegean Sea.

The results of this MSc thesis from the raw data of these marine records and their comparison to the simulated data of temperature and precipitation can strengthen the existing models.

Key words: Paleoceanography, North Aegean, Foraminiferal analysis, PaleoClimate Model Reconstructions

ΠΕΡΙΛΗΨΗ

Κατά τη διάρκεια των τελευταίων δεκαετιών, πληθώρα επιστημονικών μελετών υποστηρίζουν και αναδεικνύουν τη μελέτη των μικροαπολιθωμάτων σε συνδυασμό με την ανάλυση των γεωχημικών δεικτών στα θαλάσσια ιζήματα ως εξαιρετικό εργαλείο για την ανασύσταση των παλαιοωκεανογραφικών συνθηκών και την ιστορία του παλαιοκλίματος. Σήμερα, η συγκριτική ανάλυση δεδομένων από τα θαλάσσια ιζήματα με δεδομένα από κλιματικά μοντέλα προσφέρει ακόμα περισσότερες πληροφορίες σχετικά με την εκτίμηση των παλαιοωκεανογραφικών και παλαιοκλιματικών διακυμάνσεων.

Η παρούσα εργασία έχει ως αντικείμενο την παλαιοωκεανογραφική εξέλιξη κατά τα τελευταία 4000 χρόνια του Βορείου Αιγαίου, μίας περιοχής ιδιαίτερης σημασίας λόγω των μοναδικών γεωγραφικών και ωκεανογραφικών χαρακτηριστικών της. Στο πλαίσιο αυτό πραγματοποιήθηκε διεξοδική ανάλυση παλαιοωκεανογραφικών δεικτών στο ιζηματογενές αρχείο δύο πυρήνων μικρού μήκους M2 (λεκάνη του Άθω) και M3 (λεκάνη της Σκύρου) και σύγκριση των αποτελεσμάτων με τη χρήση δεδομένων από παλαιοκλιματικά μοντέλα στην περιοχή ενδιαφέροντος.

Κατά την ανάλυση κατεγράφησαν οι διακυμάνσεις της παλαιοθερμοκρασίας των επιφανειακών υδάτων από δεδομένα αλκενονών για το διάστημα 1.600 - 600 π.Χ. (πυρήνας μικρού μήκους M3). Επίσης, ο προσδιορισμός των διακυμάνσεων σε διάφορες παλαιοωκεανογραφικές παραμέτρους κατά τη διάρκεια των τελευταίων 1500 χρόνων (πυρήνας μικρού μήκους M2) επιτεύχθηκε με στοιχεία των σταθερών ισοτόπων ($\delta^{18}O$ και $\delta^{13}C$) που μετρήθηκαν σε κελύφη του πλαγκτονικού τρηματοφόρου *Globigerinoides ruber* και την εφαρμογή του δείκτη χαμηλής οξυγόνωσης (LO, Low Oxygen) των βενθονικών τρηματοφόρων που εκφράζει τις μεταβολές στη συγκέντρωση του διαλυμένου οξυγόνου στα ύδατα του πυθμένα σε συνδυασμό με την καταγεγραμμένη

θερμοκρασία των επιφανειακών υδάτων από δεδομένα αλκενονών και το δείκτη στρωμάτωσης της υδάτινης στήλης (S-index) των κοκκολιθοφόρων.

Τα δεδομένα της θερμοκρασίας των επιφανειακών υδάτων με βάση τις μετρήσεις των αλκενονών αντιπαραβλήθηκαν με προσομοιώσεις θερμοκρασίας και βροχόπτωσης που πραγματοποιήθηκαν από κλιματικά μοντέλα του Coupled Model Intercomparison Project (CMIP5) για τα τελευταία 2000 χρόνια. Ειδικότερα, οι προσομοιώσεις των MPI-ESM-P-p2k, MPI-ESM-P r1 και CCSM4 r1 για τη συγκεκριμένη περιοχή αναλύθηκαν σε ετήσια και εποχική ανάλυση. Σύμφωνα με τα αποτελέσματα αυτής της μεταπτυχιακής διπλωματικής διατριβής η μελέτη των πρωτογενών δεδομένων καθώς και της σύγκρισής τους με τις προσομοιώσεις θερμοκρασίας και βροχόπτωσης μπορεί να συμβάλει στην ενίσχυση των ήδη υπαρχόντων παλαιοκλιματικών μοντέλων.

Λέξεις Κλειδιά: Παλαιοωκεανογραφία, Βόρειο Αιγαίο, Τρηματοφόρα, Παλαιοκλιματικά μοντέλα

1 INTRODUCTION

1.1 Paleoceanographic reconstructions

Although the anthropogenic impacts in the last era are likely to be a dominant influence on climate, natural forcing mechanisms (solar, volcanic and orbital) direct in the climate system as well (Stott, 2000). The research of pre-instrumental period provides a baseline of investigation in order to improve the attribution of climate change to natural and anthropogenic forcing (Schurer et al., 2013). Evidence of past forcing is preserved in a wide range of natural archives, including ice sheets, stalagmites, corals, tree rings, marine and lake sediments that provides the basis for reconstructing paleo climates and information about changes in the atmosphere, ocean, cryosphere, biosphere as well as their interactions. The virtual baseline of knowledge about the past will provide the context for forecasts of future climatic variations in regional as well as global -scale (Alverson et al., 1999; Bradley and Eddy, 1991).

The oceans comprise over 70% of the earth's surface and are intimately linked to present and past climate global scale. The ability of ocean water to absorb, store and transport heat gives it an active and dynamic role in determining the state of the earth climate. Marine sediments preserve a number of physical, chemical and biological proxy indicators that reflect the climatic and oceanographic environment and can therefore be applied to reconstruction of paleoclimatic and paleoceanographic evolution. These paleoceanographic proxy indicators provide evidences of past changes on a number of parameters such as temperature, salinity, productivity, circulation patterns, deep-water ventilation, nutrient cycles, oxygen content, etc. Among them, Sea Surface Temperature (SST) and Sea Surface Salinity (SSS) are the most important oceanographic parameters linked to many atmospheric and oceanic processes. Their variations are driven by precipitation and evaporation, and their patterns control seawater density, which is the major factor governing the ocean circulation.

The proxy data which can reveal the observational features of the past climate and environmental conditions and paleo simulations using ocean and climate models which can provide a baseline of understanding the mechanisms of the past climate change

constitute two common approaches of paleoceanographic reconstructions. However, the contemporaneous analysis of both proxy data- model-derived records obviously can contribute to increased information about the evaluation of past climate variability.

1.1.1 Proxy data

In paleoceanographic research, a large number of biotic and abiotic proxy techniques have been established, providing a valuable insight into past conditions (Bradley, 1999); (Fischer and Wefer, 1999); (Wefer G. et al., 1999); (Henderson, 2002);(Cowie, 2013). The most widespread used paleoceanographic proxies include the microfossil assemblages, stable oxygen and carbon isotopes, as well as alkenones.

Microfossil assemblages

The main marine microfossil groups include foraminifera and coccolithophores (calcareous), radiolarians, silicoflagellates, and diatoms (siliceous) and organic-walled dinoflagellates. Their abundance, diversity and species distribution is highly dependent on ecological parameters. Coccolithophores, diatoms, silicoflagellates and dinoflagellates constitute the majority of the marine eukaryotic phytoplankton and their distribution reflect even small changes in conditions of upper photic zone, such as SST, SSS and nutrient availability (McIntyre and Bé, 1967); (Knappertsbusch, 1990); (Kleijne, 1993); (Boyd and Doney, 2002); (Reynolds, 2006); (Holzwarth et al., 2010); (Malinverno et al., 2016). The geographically and bathymetrically distribution of zooplankton such as planktonic foraminifera and radiolarians are tightly linked to ocean temperature, salinity and productivity (Hemleben et al., 1989); (Pujol and Vergnaud Grazzini, 1995); (Boltovskoy, 1998); (Bradley, 2015). Benthic foraminifera represent the most important contributors to the meiofauna and their distribution is strongly controlled by water mass characteristics, such as temperature, salinity, dissolved oxygen and the flux of particulate organic matter from the upper ocean to the sea floor (Corliss, 1980); (Murray, 1991); (Altenbach and Struck, 2001; Gooday, 1994, 2003; Jorissen, 1999); (Pawlowski and Holzmann, 2008). Consequently, the relative abundance of different species contained in a fossil assemblage have been widely applied for establishing environmental and climatic

reconstructions (Baumann et al., 1999 ; Sangiorgi et al., 2002); Pawlowski and Holzmann, 2008 ; Vink et al., 2000 ; Jorissen et al., 2007 ; de Vernal et al., 2005; de Vernal et al., 2000 ; Triantaphyllou et al., 2009a ; Triantaphyllou et al., 2014; Triantaphyllou et al., 2016).

Moreover, wide arrays of marine biotic indices based on related changes in microfossil assemblage data are highly applied to reconstruct paleo-environments in paleoceanographic and paleoclimatic studies. In this respect, the S index for evaluating the stratification of the upper water column based on coccolithophores (Triantaphyllou et al., 2009a), and the Low Oxygen (LO) index for evaluating the changes in bottom water oxygenation based on benthic foraminifera assemblages (Kuhnt et al., 2007) are among the commonly used indices.

Stable oxygen and carbon isotopes

High-resolution time series of stable oxygen and carbon isotopic analyses ($\delta^{18}O$ and $\delta^{13}C$) of the calcite tests produced by foraminifera and also corals or bivalves are widely used for the reconstruction of past climates and ocean conditions (Vergnaud-Grazzini, 1985 ; Negri et al., 1999 ; Rohling and Cooke, 1999 ; Bernasconi and Pika-Biolzi, 2000 ; Kuhnt et al., 2008 ; Grauel et al., 2013b ; Margaritelli et al., 2016 ; Triantaphyllou et al., 2016).

The isotopic composition of foraminiferal tests is dependent on physical conditions and composition of ambient seawater in which they calcify. In general, $\delta^{18}O$, as well as $\delta^{13}C$ of planktonic and benthic foraminiferal tests have been used as tracers to reconstruct past ocean surface and bottom-water conditions respectively. The sea water oxygen isotope ratio is linked with fractionation processes within the hydrological cycle; therefore measured $\delta^{18}O$ can provide information on past variations in temperatures, ice volume changes, salinity effect, and so precipitation-evaporation rates and freshwater input changes. In contrast, the carbon isotope ratio of sea water is intimately controlled by the physiological processes, principally photosynthesis and respiration; consequently

measured $\delta^{13}C$ can be used to estimate paleoceanographic parameters such as marine productivity, past ocean circulation and carbon cycle changes.

Alkenones

The most successful applied geochemical SST proxy in various marine settings is the lipid $U^{K'}_{37}$ index based on long-chain, unsaturated methyl and ethyl ketones known as alkenones (Emeis et al., 1998); (Cacho et al., 2001); (Herbert, 2003); (Martrat et al., 2004); (Gogou et al., 2007; Gogou et al., 2016); (Triantaphyllou et al., 2009b); (Moreno et al., 2012); (Grauel et al., 2013a); (Nieto-Moreno et al., 2013).

Alkenones are biosynthesized by phytoplankton mainly the coccolithophore *Emiliana huxleyi* and the closely related *Gephyrocapsa oceanica* (Volkman et al., 1980 ; Marlowe et al., 1984). Both species are the most abundant and widespread in the upper photic zone of modern oceans and particularly respond rapid to changing temperature conditions. Alkenones record a temperature signal that reflects the surrounding water temperature in which they are produced. A global calibration of the alkenone unsaturation index from surface sediment samples has shown a robust and linear relationship between the $U^{K'}_{37}$ and the mean annual SSTs (Müller et al., 1998 ; Conte et al., 2006). Because they are among the most resistant to degradation lipid (Marlowe et al., 1990; Marlowe et al., 1984) have a much high preservation capability in marine sediments and therefore is one of the most reliable tool for paleoceanography.

1.1.2 Climate Model Simulations

Climate models are powerful tools that help us to understand climate processes in past, present and future. The interpretation of their results requires a basic familiarity with their structure, the underlying assumptions (physical and numerical) (IPCC, 2007). Details on model simulations are important when comparing paleoclimate data with proxy reconstructions especially due to the different spatial and temporal scales of models and proxy reconstructions (Luterbacher et al., 2012); (Lohmann et al., 2013).

Climate models, being a computer code that can generate virtual climates similar to the observed climate, provide the means to conduct numerical experiments under changed controlled conditions, to test hypothesis similarly as it is done in the laboratory. In addition, they can also provide long, comprehensive and gap-less climatic time series covering several millennia that share some statistical properties with observed records.

The contribution of internal variability is larger at small spatial scales and short temporal scales, whereas external driven variability becomes more relevant at larger spatial scales and longer temporal scales (Bierstedt et al., 2016). At small and short scales, e.g. a few tenths of kilometers and a few weeks, weather noise is more important than the slowly changing external global drivers, such as total solar irradiance, volcanism, orbital changes (IPCC, 2013). Furthermore, a climate paleoproxy usually records local climate conditions, whereas a model grid-cell typically represents the mean conditions over 100 km of longitude and latitude.

With unlimited computer resources, many simulations could be run with different initial conditions, thus producing a range of possible trajectories that would encompass the uncertainty range, but this is in practice not possible. Once the initial conditions are prescribed, the climate model also expects the values of the external forcings for each year (solar irradiance, atmospheric concentrations of carbon dioxide and methane, volcanic aerosols, land-use changes, etc. (Schmidt et al., 2011) through the period covered by the simulation.

1.2 Paleoceanographic evidence for the last 4000 years

The Holocene is considered as a period of relatively stable climatic conditions compared to previous geological periods. However, it is marked by a series of multi-centennial to millennial scale climate oscillations that may contribute to better understanding of short-scale climate variability (e.g., Mayewski et al., 2004). During the last 4000 years, the combination of proxy records from several paleoclimate archives has enabled the recognition of the following paleoclimate phases: the Bronze Age (BA), Iron Ages (IA), Roman Warm Period (RWP), Dark Ages (DA), Medieval Climate Anomaly (MCA), Late Antique Little Ice Age Period (LALIA), Little Ice Age (LIA) and the recent instrumental Period (e.g., (Mayewski et al., 2004); (Luterbacher et al., 2012); (Büntgen et al., 2016); (Margaritelli et al., 2016); (Toohey et al., 2016). The main mechanisms to explain the late Holocene climatic variations include external forcings (e.g., solar, volcanic) and internal variability (e.g., atmosphere-ocean feedbacks like El Ninõ-Southern Oscillation -ENSO) (e.g., (Bond et al., 2001); (Mayewski et al., 2004). However, much of these climate variations are characterized by regional variability in timing, location and magnitude, resulting in a complex spatial pattern of regional and seasonal variation, presumably reflecting interactions between low- and high- latitude climate changes (Mayewski et al., 2004); (Wanner et al., 2008).

The Mediterranean basin situated in a transition zone between tropical and mid-latitude climates, is influenced by some of the most relevant mechanisms acting upon the global climate system in the modern as the well as the past times (Xoplaki, 2002). Therefore, Mediterranean region is offering a rich combination of long, high quality archives for investigation of paleoceanographic and paleoclimatic changes (Luterbacher et al., 2012); (Rohling et al., 2015). According to a review of Luterbacher et al. (2012) that summarized existing paleo-information from different marine and continental Mediterranean archives during the last two millennia, (Gogou et al., 2016) recognized the following alternating warm-cold climate phases: a humid period (RWP) for the first 300 years, a cold interval (DA) from 300 to 600 AD with a marked drop in temperatures at 450 AD, a period from 600 to 1200 AD (MCA) characterized by warmer conditions, but

interrupted by two cooler events at 700 and 1100 AD and the interval from 1200 to 1850 AD, LIA, with cooling extremes occurring at around 1400 AD and 1625 AD.

Table 1-1: Succession of paleoclimatic phases recognizable in the Mediterranean area during the last four millennia.

Nieto-Moreno (2012) Alborean Sea		**Nieto-Moreno (2011) Balearic basin**		**Lirer et al. (2014) Tyrrhenian Sea**		**Margaritelli et al. (2016) Tyrrhenian Sea**		**Grauel et al. (2013) Ionian Sea**		**Goudeau et al. (2015) Ionian Sea**		**Piva et al. (2008) Adriatic Sea**		**Gogou et al. (2016) Aegean Sea**	
Proxy data: alkenone-SST, geochemistry		Proxy data: geochemistry		Proxy data: Planktonic and benthic forams, $\delta^{18}O_{G.ruber}$,		Proxy data: Planktonic forams, $\delta^{18}O_{G.ruber}$, $\delta^{13}C_{G.ruber,}$ pollen,		Proxy data: TOC, alkenone-SST, $\delta^{18}O_{G.ruber}$, $\delta^{18}O_{Umediterranea}$		Proxy data: $\delta^{18}O_{G.ruber}$, $\delta^{13}C_{G.ruber,}$ *H. balthica* Mg/Ca		Proxy data: Planktonic and benthic forams, $\delta^{18}O_{G.bulloides}$		Proxy data: TOC, alkenone-SST, $\delta^{13}C_{org}$, organic geochemistry, pollen, coccos	
paleo clim. phase	Age (yr.AD)	paleo clim. phase	Age (yr.AD)	paleo clim. phase	Age (yr.AD)	paleo clim. phase	Age (yr.AD)	paleo clim. phase	Age (yr.AD)	paleo clim. phase	Age (yr.AD)	paleo clim. phase	Age (yr.AD)	paleo clim. phase	Age (yr.AD)
				modern warm P	1940AD upwards	modern warm P	1950AD upwards			present	1958AD-1904AD				
Inst P	1800AD upwards			Inst P	1940AD-1850AD	Inst P	1850AD-1950AD							Inst P	1850AD upwards
LIA	1800AD-1300AD	LIA	1800AD-1300AD	LIA	1850AD 1240AD	LIA	1850AD-1250AD	LIA	1850AD-1400AD	LIA	1850AD-1400AD	LIA	1840AD-1400AD	LIA	1850AD-1200AD
MCA	1300AD-800AD	MCA	1300AD-800AD	MCA	1240AD-840AD	MCA	1250AD-860AD	MCA	1200AD-800AD	MCA	1200AD-800AD	MCA	1200AD-600AD	MCA	1200AD-600AD
DA	800AD-300AD	DA	800AD-350AD	DA	840AD-530AD	DA	860AD-550AD	DA	750AD-500AD			DA	600AD-350AD	DA	600AD--bottom
RWP	300AD-650BC	RWP	350AD-650BC	RWP	530AD -bottom	RWP	550AD-500BC	RWP	200AD-1AD	RWP	450AD-0AD	RWP	350AD-100BC		
		IA / Late BA	650BC-1650BC			IA / middle BA	500BC-1900BC					IA	100BC-1500BC		

Despite that only few studies are available, derived from scattered cores around the Mediterranean region, the marine environment appears to have a clearly response to the late Holocene climate oscillations (e.g., (Schilman et al., 2011); (Sprovieri et al., 2010); (Piva et al., 2008a); (Incarbona et al., 2008); (Incarbona et al., 2010); (Nieto-Moreno, 2012; Nieto-Moreno et al., 2011); (Grauel et al., 2013a); (Lirer et al., 2014); (Goudeau et al., 2015); (Gogou et al., 2016); (Margaritelli et al., 2016). Paleoclimatic phases recognizable from high-resolution marine Mediterranean records for the last four millennia are presented in Table 1-1. A disagreement in the onsets of the RWP can be attributed in a non-uniform climate signal amongst the various basins (e.g., (Gogou et al., 2016). Moreover, the short-scale climate cooling of LALIA phase (Büntgen et al., 2016) was not recovered, whereas the onsets and offsets of paleoclimate phases before of the last 2000 years are more complicated because this period displays few datasets.

1.3 Scope of the present study

The scope of this thesis was to combine and compare atmospheric paleo climate model reconstructions with organic geochemical and proxy analysis (isotopic signal, dissolved oxygen concentrations, stratification index) from two high resolution marine sediment cores retrieved from the North Aegean Sea. From these we focused on the last 4000 years in order to try to interpret the dominant past climate conditions and provide even more information about the paleoceanographic and paleoclimatic conditions of the area which is sensitive to climatic and environmental changes.

2 STUDY AREA

2.1 The Mediterranean Area

The Mediterranean Sea is a marginal and semi-enclosed basin connected to the Atlantic Ocean through the narrow and shallow Gibraltar Strait (width 14.5 km; depth less than 300m). To the northeast, it is connected with the Black Sea by the Dardanelles and Bosphorus straits. The Strait of Sicily subdivides the sea into main basins, the Western Mediterranean (WMED) and the Eastern Mediterranean (EMED). The WMED contains the Alboran, the Balearic, the Ligurian and the Tyrrhenian Seas, whereas the EMED that is characterized by more complicated topography than WMED, comprises the deep Ionian and Levantine basins and the Adriatic and Aegean shelf seas (Figure 2.1).

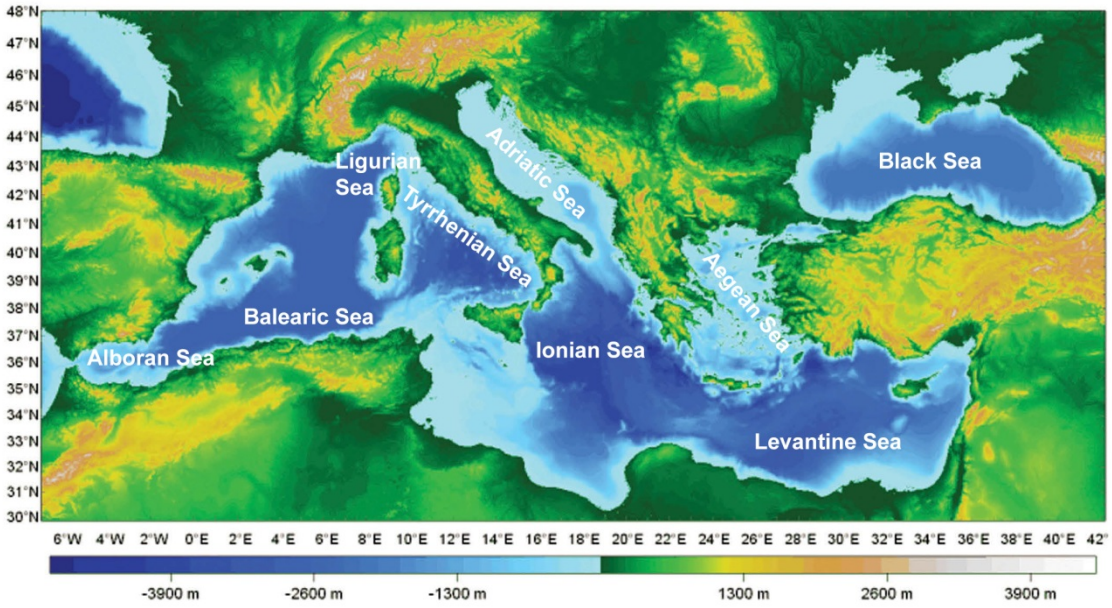

Figure 2.1: Orographic and bathymetric map of the Mediterranean region (http://www.unipv.it/cibra/MedBathy%20800.gif).

The Mediterranean Sea is characterized by a highly complex and variable circulation pattern, strongly affected by several driving forces, strong topographic constraints, and internal dynamic processes (Robinson et al., 1991). The thermohaline circulation of the

surface layer in the Mediterranean Sea is dominated by the eastward path of low-salinity Atlantic Water (AW). In the intermediate layers, the Levantine Intermediate Water (LIW) in the Levantine Basin, and the Cretan Intermediate Water (CIW) in the Cretan Sea are formed by vertical mixing during winter (Roether et al., 2007); (Bergamasco and Malanotte-Rizzoli, 2010; Malanotte-Rizzoli et al., 1997). The transformation of AW into LIW occurs through surface heat loss and evaporation specifically in the Levantine basin (Figure 2.2).

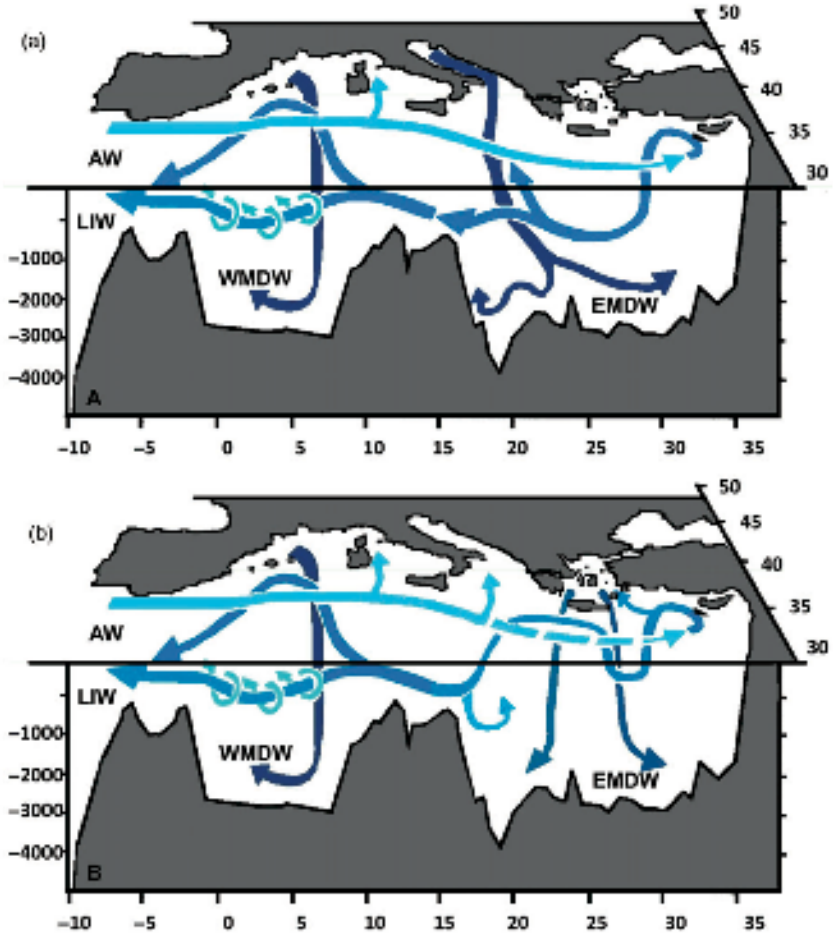

Figure 2.2: Mediterranean Sea Thermohaline Circulation Scheme. Note the Eastern Mediterranean behaviour before (upper panel) and during (bottom panel) the Eastern Mediterranean Transient (EMT) (Bergamasco and Malanotte-Rizzoli, 2010).

The Western Mediterranean Deep Water (WMDW) and the Eastern Mediterranean Deep Water (EMDW) are formed in the deep layers. In the EMED the source of the EMDW is the Southern Adriatic, but temporarily moved to the Aegean/Cretan Sea during the

Eastern Mediterranean Transient (EMT) event (Roether et al., 1994), 2007; Malanotte-Rizzoli et al., 1999; Theocharis et al., 2002;(Bergamasco and Malanotte-Rizzoli, 2010).

The Mediterranean Sea is located in a transitional climatic zone, where tropical and mid-latitude variability, making it highly sensitive to the global climate change (Corte-Real et al., 1995; Lionello et al., 2006; Ribera et al., 2000; Xoplaki et al., 2003a). The climate of the Mediterranean area is strongly affected by the complex topography, orography, land-sea distribution and large-scale mid-latitude atmospheric circulation such as the Arctic Oscillation/North Atlantic Oscillation (AO/NAO) and other teleconnection patterns (Gogou et al., 2016; Xoplaki et al., 2003a).

The Mediterranean Sea is a concentration basin, where evaporation exceeds precipitation. Today it is characterized by a strong seasonal climate pattern, with warm to hot, dry summer and mild wet season between October to March (Xoplaki, 2002). However, warming (Figure 2.3) and increased drought (Figure 2.4) show significant trends in recent years (e.g.,(Giorgi, 2002a); (Camuffo et al., 2010); (Hoerling et al., 2012); (Skliris N. et al., 2012) and model projections indicate an rise in average temperatures and reduction in annual precipitation (e.g. (Giorgi and Lionello, 2008); (Nikulin et al., 2011). Nevertheless, climate variability at sub-regional scale is high and trends in many regions are statistically non-significant in view of the large variability (e.g., Xoplaki, 2002).

The Mediterranean region offers a rich combination of long, high- quality instrumental time series, natural archives, and documentary information across time and space, making possible sufficiently sensitive reconstructions of climate in past centuries (Luterbacher et al., 2012).

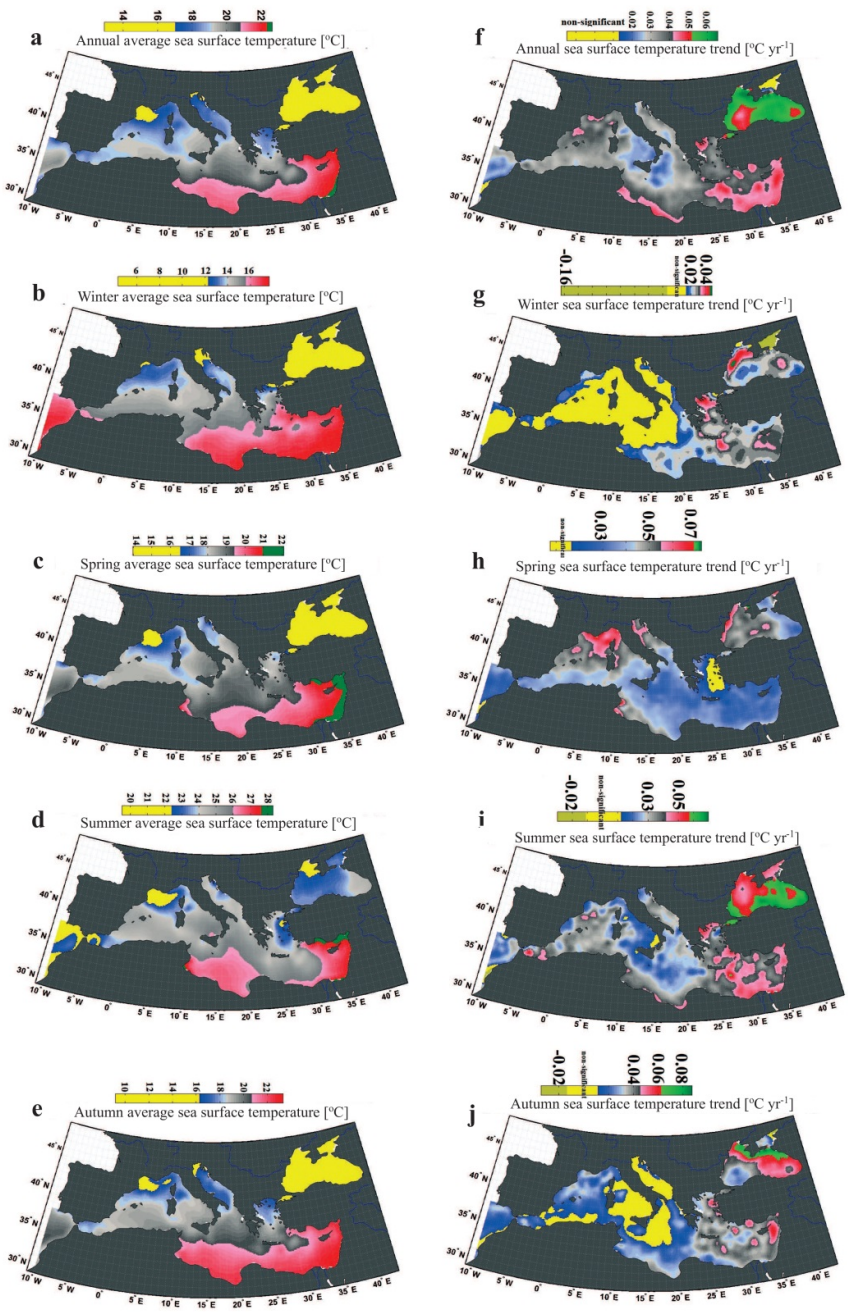

Figure 2.3: Spatial distribution of annual/seasonal Sea Surface Temperature (SST) means and trends over the 1982–2012 period (Bergamasco and Malanotte-Rizzoli, 2010).

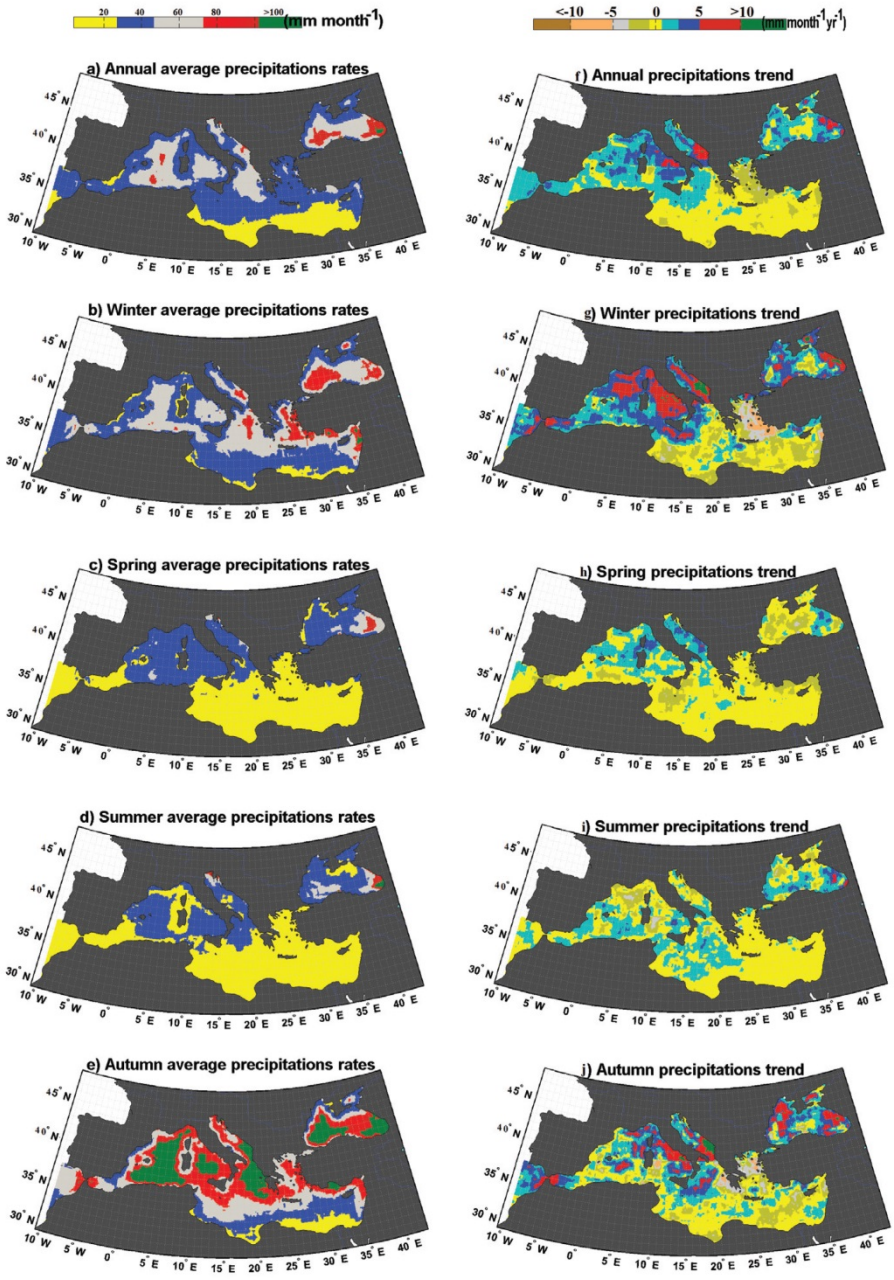

Figure 2.4: Spatial distribution of annual/seasonal precipitation rates, means, and trends over the 1998–2010 period in the Mediterranean and adjacent sub-basins (Bergamasco and Malanotte-Rizzoli, 2010).

2.2 The Aegean Sea

The semi-enclosed Aegean Sea is located in the northeastern region of the Mediterranean and is linked to the Black Sea through the Dardanelles and Bosphorus straits and to the eastern Mediterranean through the Cretan Straits. The basin formed in a back-arc setting

related to the Hellenic subduction system was active since at least the Late Cretaceous (e.g., (Le Pichon and Angelier, 1979); (Horvath and Berckhemer, 1982); (Robertson et al., 1991). The Aegean area is characterized by a complex morphology as a result of the geological history and the recent tectonic and geodynamic evolution. Based on morphological characteristics as well as geotectonic regimes it can be divided into three distinct but communicating and interacting sub-basins (northern, central and southern) (Figure 2.5).

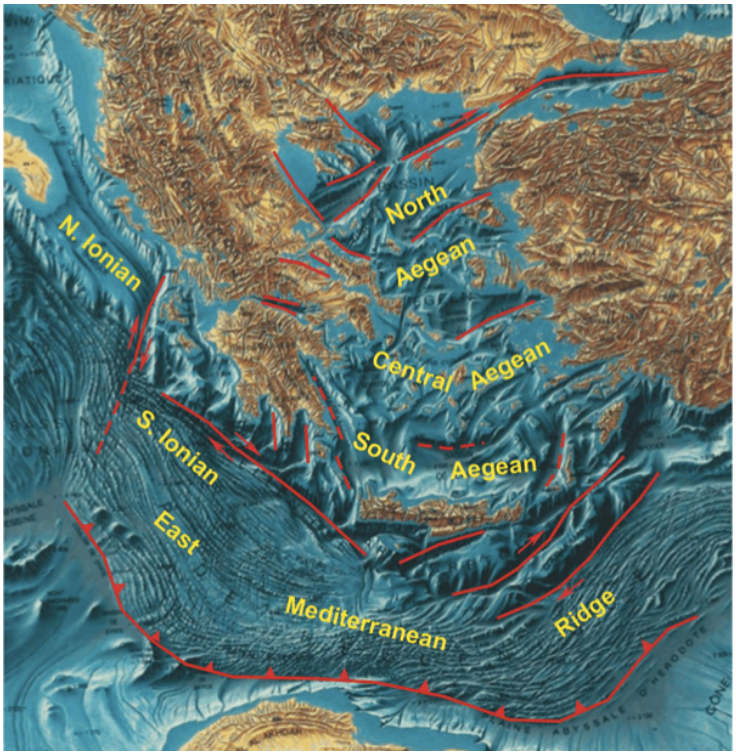

Figure 2.5: Relief map of the Hellenic region with main geotectonic features and names of morphologic domains (SoHelME, 2005).

The Aegean Sea is featured by an overall cyclonic upper thermohaline circulation (Lykousis et al., 2002). In general it is characterized by low precipitation and elevated salinities associated with high evaporation rates. However, Sea Surface Salinity (SSS) as well as Sea Surface Temperature (SST) show strong seasonally and important gradients from north to south. The annual maximum SST (~24 ◦C) occurs around August/September, and minimum SSTs (~13 ◦C) follow in February/March (Dimiza et

al., 2016; Poulos et al., 1997; Triantaphyllou et al., 2004), whereas SSS values vary between 31‰ to 39‰.

The Aegean basin generally represents an oligotrophic region (Ignatiades et al., 2002). The South Aegean sub-basin is characterized by very low export rates of organic carbon from the surface layer, and organic-poor sediments (Gogou et al., 2000); coccolithophores are one of the major primary producers in this ecosystem ((Ignatiades et al., 2002); Triantaphyllou et al. 2004; Dimiza et al., 2015).

2.2.1 North Aegean Basin

The Northern Aegean Sea is characterized by the Northern Aegean Trough (NAT), which has developed along the trace of the Northern Anatolian Fault (NAF) (Lyberis, 1984). The NAT comprises a series of three main SW-NE oriented depressions (down to a depth of 1500 m), separated by morphological highs (Figure 2.6).

Figure 2.6: Bathymetric map of the Hellenic Seas (depths in meters) and location of major morphological features (SoHelME, 2005).

The physical oceanography of the North Aegean Sea is controlled not only by the regional climate but also the complicated physical and geographic configuration, displaying complicated seabed morphology and numerous island complexes. The freshwater discharges from rivers from the north Hellenic coast and the eastern Turkish coastline and seasonal variation in input rates of Black Sea surface water through the Strait of Dardanelles supply the northern Aegean with freshwater inputs (Poulos et al., 1997); (Roussakis, 2004);(Triantaphyllou et al., 2016). The cooler (9–22°C) and low salinity (24–28‰) surface Black Sea Water (BSW) outflowing through the Dardanelles Strait flows to the southwest Aegean Sea along the east coast of Greece, enhancing the productivity of the North Aegean Sea. Warmer (16–25°C) and highly saline (39.2–39.5‰) Levantine Surface Water (LSW) occupies surface layers in the absence of BSW, and LIW (14–15 °C, 38.8–39.1‰) extends to a depth of up to about 400 m below the BSW/LSW. These water masses flow northwards along the eastern Aegean as far as the Dardanelles Strait (Zervakis et al., 2000). The region hosts the main source area of new deep water formation in the eastern Mediterranean (Theocharis et al., 1999); (Zervakis et al., 2000); (Velaoras and Lascaratos, 2005); (Androulidakis et al., 2012; Velaoras and Lascaratos, 2005; Zervakis et al., 2000).

3 MATERIALS AND METHODS

3.1 Core description and chronology

The multicore M2 (40° 05.15´N, 24° 32.68´E) was recovered from the Athos basin, North Aegean Sea, Greece at a water depth of 1018 m, whereas the multicore M3 (39° 15.71´N 24° 59.93´N) was retrieved from the Skyros basin North Aegean Sea, Greece at a water depth of 800 m, during the 'MEDECOS II' cruise onboard the R/V 'Aegaeo' in 2010 (Figure 3.1,Figure 3.2). Both cores were sampled continuously at a sampling step of 0.5 cm. They consist of olive grey (2.5GY 5/1) to greyish olive (5Y 5/2) homogeneous mud, with high silt contents (25 to 45%); 40–60% of the total material is comprised mostly of illite (lithologic unit A; (Roussakis, 2004).

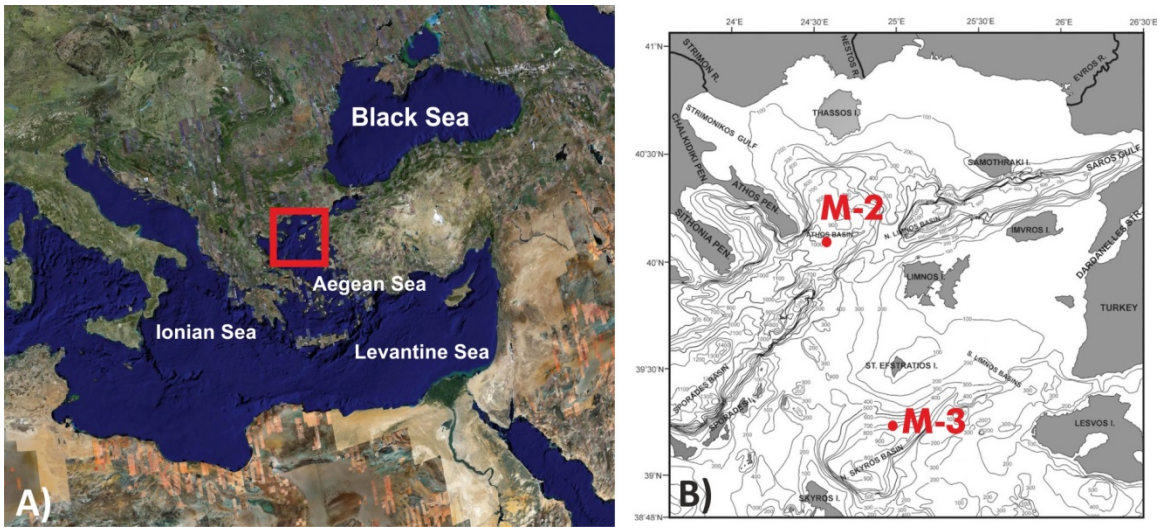

Figure 3.1: (A) Location of the study area, (B) M2 and M3 cores locations.

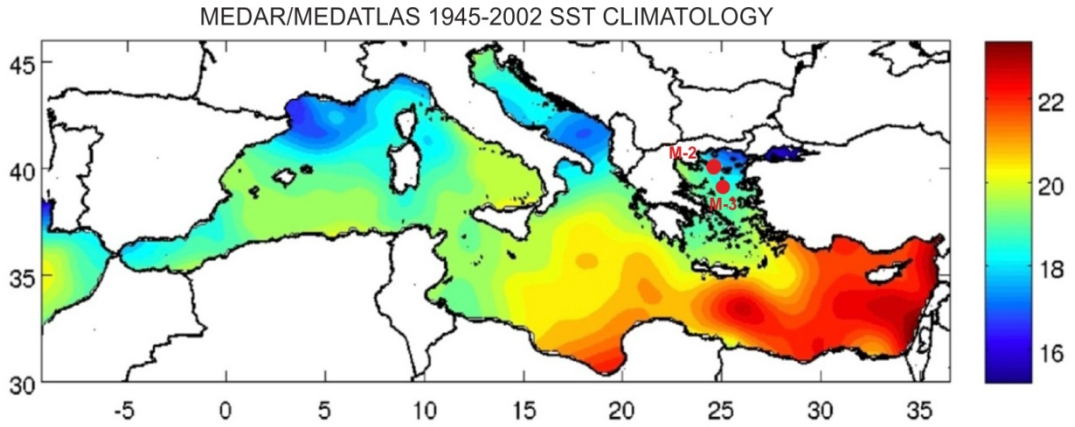

Figure 3.2: Location of the study area in the north Aegean Sea. Mean SSTs calculated from 1945 to 2002 period using the MEDAR/MEDATLAS 2002 database (Fichaut et al., 2003) (from Gogou et al., 2016).

The age-depth model for multicore M2 has been established by combining ^{210}Pb dates and calibrated AMS (accelerator mass spectrometry) ^{14}C dates (Table 3-1) (Gogou et al., 2016). ^{210}Pb measurements were performed on the upper 10 cm at a step of 0.5 cm; the resolution became 1 cm until 20 cm depth, and increased up to 5-10 cm until 40 cm depth. ^{210}Pb activity profile were presented in Gogou et al. (2016); (Figure 3.3). AMS ^{14}C analysis was performed on 5 samples through Beta Analytic Inc., USA. The dates have been calibrated using a regional marine reservoir correction of 58 ± 85 years (Reimer and McCormac, 2002). A sedimentation rate of the order of 83cm/kyr, was obtained from the ^{210}Pb analysis, which is close to the ~87 cm/kyr estimate derived from the ^{14}C dating for the 0-17 cm interval. The age of other levels in the core is based on linear interpolation between the ^{14}C dates assuming constant sedimentation rates.

Table 3-1; Age model pointers for the investigated core M2. (*) result is out of calibration range (Gogou et al., 2016).

depth (cm)	material	^{14}C ages	cal year BP	cal year AD	mean age	error ±1σ
16.5-18.5 cm	planktonic forams	200±30$^{(*)}$		1750	1750	21
23.5-25.5 cm	planktonic forams	760±30	271-440	1510-1679	1594.5	60
30.5-32.5 cm	planktonic forams	950±30	440-570	1380-1510	1445	46
41.5-43.4 cm	planktonic forams	1520±30	919-1116	834-1031	932.5	70
46.5-48.5 cm	planktonic forams	1910±30	1309-1496	454-641	547.5	66

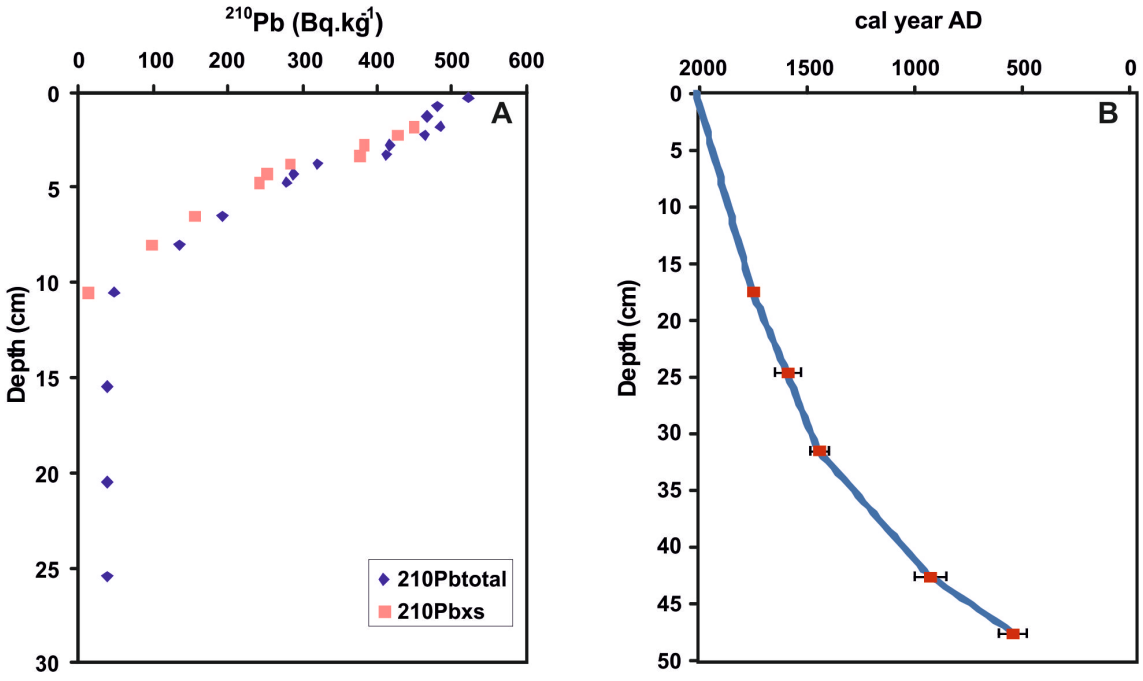

Figure 3.3: Information used to construct age model. (A) ^{210}Pb activity downcore M2 core, and (B) depth vs. AD ages (with 1s error) for M2 core (Gogou et al., 2016).

The age model for multicore M3 is based on linear interpolation between five AMS datings (Figure 3.2).

Table 3-2: Age model pointers for the investigated core M3.

depth (cm)	material	^{14}C ages	cal year BP	cal year AD	mean age	error ±1σ
44	planktonic forams	3900+/-30	3674-3918	1969-1725	1847	87
38	planktonic forams	3720+/-30	3452-3679	1730-1503	1616.5	81
29	planktonic forams	3170+/-30	2773-2992	1043-824	933.5	78
23	planktonic forams	3010 +/- 30	2638-2844	895-689	792	73
16	planktonic forams	2860 +/- 30	2436-2680	731-487	609	87

3.2 Alkenone-based Sea Surface Temperatures (SSTs)

Estimates of past Sea Surface Temperature (SST) were calculated on 96 samples by means of the unsaturation ratios of alkenones ($U=C_{37:2}/(C_{37:2} + C_{37:3})$ and the global calibrated parameters (Conte et al., 2006):

$$\left(T = -0.957 + 54{:}293(U) - 52.894(U)^2 + 28.321(U)^3\right)$$

The analytical precision is better than 0.6 ^{o}C. For alkenone based SST records from multicore M2 we use data previously published in Gogou et al. (2016). The alkenone record from M3 was calculated and analysed at the Hellenic Centre for Marine Research (HCMR) under the supervision of Dr. Alexandra Gogou.

3.3 Foraminiferal analysis

For foraminiferal analysis, the multicore M2 were sampled with a spacing of 0.5 cm. Ninety five sediment samples of approximately 2 g dry weight were disintegrated by hydrogen peroxide and then sieved through a 125 μm mesh.

3.3.1 Isotope analyses ($\delta^{13}C$ and $\delta^{18}O$)

$\delta^{13}C$ and $\delta^{18}O$ ratios were measured in the planktonic foraminifer *Globigerinoides ruber* (*alba*). This typical subtropical taxon is common in the warm and oligotrophic surface waters of the eastern Mediterranean (Pujol and Vergnaud Grazzini, 1995).

Forty samples consisting of six tests of *G. ruber* (*alba*) each (>125 μm) were cleaned prior to analysis. The isotope measurements were carried out at the Stable Isotope

Laboratory Department of Earth & Planetary Sciences, University of California, Davis. Isotope results are reported as per mil, or parts per thousand (‰), standardised to Vienna Pee Dee Belemnite (VPDB). The VPDB standard is a hypothetical material recognized by the International Atomic Energy Agency (IAEA) to ensure abundances of stable isotopes are reported on the same scale and can be correlated globally (Coplen, 1994). Repeat analysis was done on three of the samples. The $\delta^{13}C$ analyses had standard deviation of 0.40, whereas $\delta^{18}O$ had standard deviations, up to 0.37.

3.3.2 Benthic foraminifera - Low Oxygen (LO) index

The analysis of the benthic foraminiferal fauna was carried out on 95 samples of the >125 m size fraction. In each case, a subset containing approximately 300 benthic foraminifera was obtained using an Otto microsplitter. All subsamples were examined under a Leica APO S8 stereoscope and specimens from each sample were picked and identified following the generic classification of Loeblich and Tappan (1987, 1994).

To evaluate the changes in bottom water oxygenation the Low Oxygen (LO) index of (Kuhnt et al., 2007) was applied. The LO index is based on the relative abundance of dysoxic and suboxic indicators. It is calculated as follows:

$$LO = (DO*0.5) + AO$$

where DO = relative abundance of dysoxic indicators (*Bolivina* spp., *Brizalina* spp., *Bulimina* spp.) and AO = relative abundance of species well adapted to suboxic and occasional anoxic conditions (*Cassidulinoides bradyi, Chilostomella oolina, Fursenkoina* spp., *Globobulimina* spp., *Nonionella* spp.: e.g., (Alavi, 1988); (Bernard and Sen Gupta, 1999; Sen Gupta and Machain-Castillo, 1993).

3.3.3 Coccolithophores - Stratification S index

Seventy three samples for coccolithophore analysis were treated according to standard procedures (Gogou et al., 2016).

Here, the ratio between *Florisphaera profunda* (F) and *Emiliania huxleyi* (E) abundances:

$$S= F/F + E$$

is applied as stratification S index of the upper water column (Triantaphyllou et al., 2014). High values in the S index (values closer to 1) indicate relatively deep nutricline/thermocline position, while low values (values closer to 0) imply high paleoproductivity (Flores et al., 2000). *Florisphaera profunda* and *E. huxleyi* generally are the dominant coccolithophores in the lower and upper photic zone of the eastern Mediterranean. In particular, the increase of *F. profunda* relative abundance is associated with decline of primary productivity of the surface waters, which shifts to the deeper layers of the water column. For S index results from multicore M2 we use data previously published in Gogou et al. (2016).

3.4 Climate Model Simulations data

In this study, we compare the annual temperature anomalies, as given from different model simulations over the last two millennium and the estimated from alkenone temperature proxy in the northern Aegean (NE Mediterranean) during the last 1500 years. Three model simulations that belong to the group of Coupled Model Intercomparison Project Phase 5 (CMIP5, (Taylor et al., 2012) were selected for comparisons with marine proxy records for SST based on alkenones from the multicore M2. Community Climate System Model, version 4 - CCSM4 r1 (National Center for Atmospheric Research) (Figure 3.4) and Max-Planck-Institute Earth System Model-Paleo - MPI-ESM-P r1

(Hamburg Max-Planck) simulations have as start date AD 850, while MPI-ESM-P p2k (Hamburg Max-Planck) begins in year 100 BC (Figure 3.5). The model simulations data analysis was held at the Justus Liebig University of Giessen under the supervision of Dr. Elena Xoplaki and Prof. Juerg Luterbacher.

The CCSM4 for this study has grid size of 36 (x size 9, y size 4) beginning at longitude E 20^{o} and latitude N 39^{o} 6' 35.6″ with horizontal resolution 1.25°.

The MPI-ESM-P model consists of the atmospheric model ECHAM6 with horizontal resolution 1.87° x 1.85° providing data for the area over the Mediterranean of 160 km longitude x 200 km latitude and 47 vertical levels. Here it has grid size of 12 (x size 6, y size 2) beginning at longitude E 20^{o} 37' 30″ and latitude N 40^{o} 6' 10.7″, N 41^{o} 58' 5.6″.

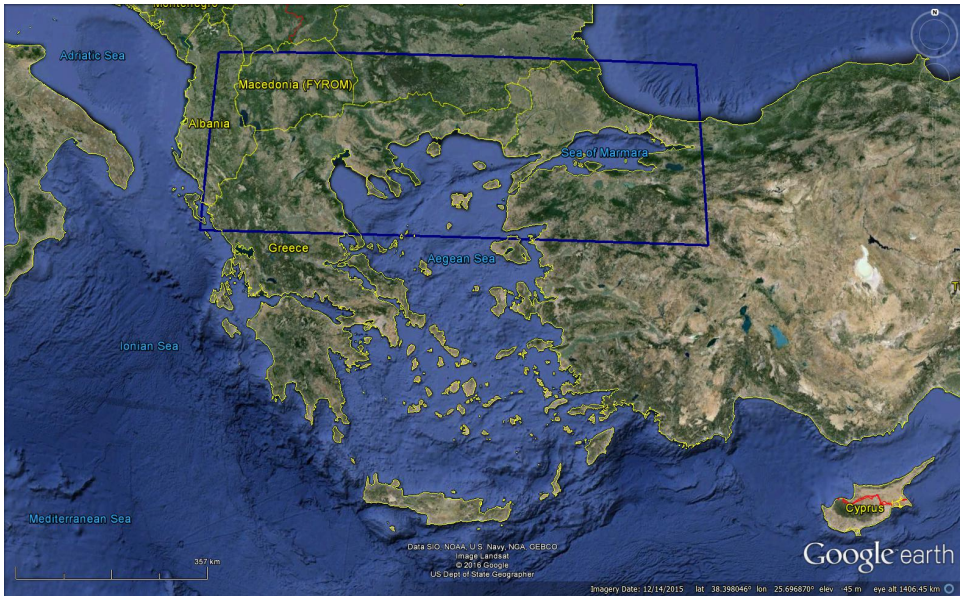

Figure 3.4: Exact geographical data domain of the Northern Aegean from CCSM4 simulation.

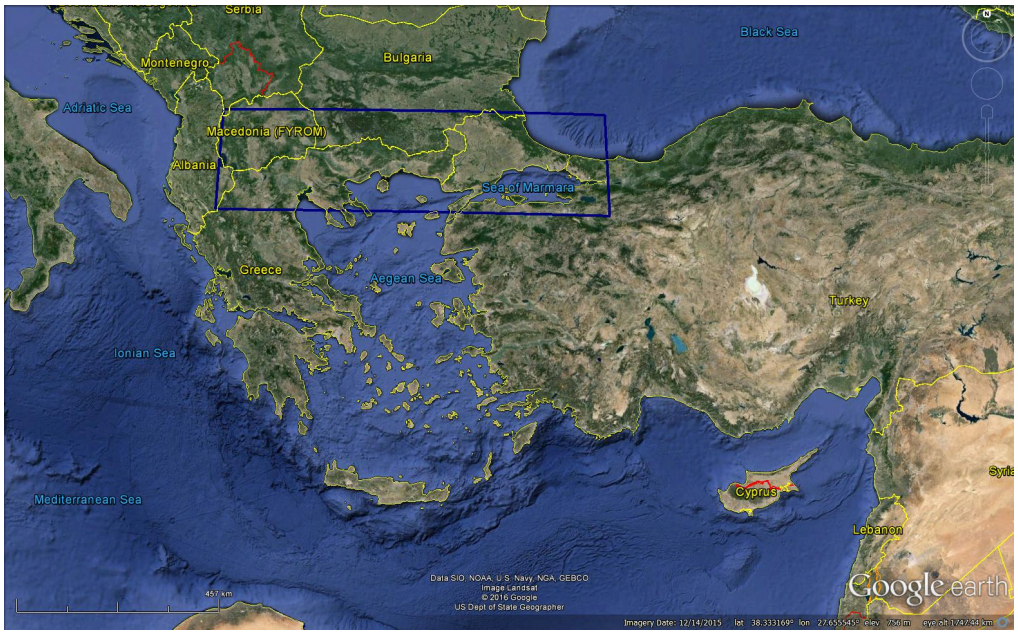

Figure 3.5: Exact geographical data domain of the Northern Aegean for the MPI-ESM-P simulation.

An important advantage of CMIP5 is the integration of idealized experiments to understand decisive climate processes like clouds, short runs starting from common initial conditions for exploring decadal prediction, and the incorporation of new model diagnostics, resulting to a better comparison of model and satellite data (Xoplaki et al., 2015). Moreover, the CMIP5 simulations have the highest spatial horizontal resolution. The experiments are based on changes of external forcing parameters (i.e., volcanic eruptions, solar variations, orbital, and anthropogenic changes in the composition of the atmosphere and land use change; (IPCC, 2013) following the Paleoclimate Model Intercomparison Project Phase III (PMIP3) protocol (Schmidt et al., 2012) (Figure 3.6). The external forcing parameters of the CCSM4 and MPI-ESM-P are related to transient changes in orbital, solar, volcanic, green-house gas and land use forcing (Schmidt et al., 2012). Both simulations used the solar irradiance reconstruction of Vieira et al., (2011).

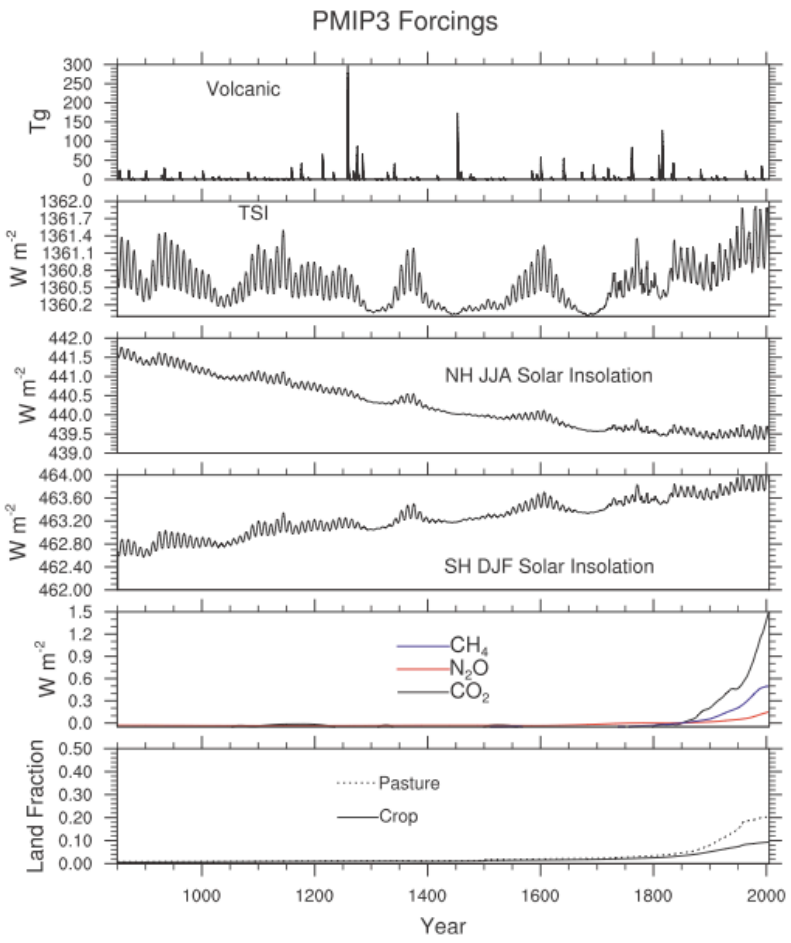

Figure 3.6: Forcings used in the ‘‘Last Millennium’’ simulation and its extension through the twentieth century to 2005 (Landrum et al., 2013).

In regards to the implementation of the volcanic forcing, CCSM4 used the volcanic forcing data (Gao et al., 2008) and MPI-ESM-P used the volcanic reconstruction of (Crowley and Unterman, 2013).

The ‘‘Last Millennium’’ (LM) simulation of the CCSM4 model consists of an atmospheric component Community Atmosphere Model, version 4 (CAM4) with 26 vertical levels and a horizontal resolution of 0.9° x 1.25° coupled with the Parallel Ocean Program (POP) (Smith et al., 2010) with a variable horizontal resolution of 1.1° increasing from 0.54° at 33° N/S towards 0.27° at the equator and 60 vertical levels. For this model only one realisation is available, however, the advantage of the simulation is

its extraordinary high spatial resolution for a Global Earth System Model, which corresponds to 80 km longitude x 140 km latitude over the Mediterranean region (Xoplaki et al., 2015). The Community Climate System Model is a general circulation climate model consisting of atmosphere, ocean, land, and sea ice components that are linked through a coupler that exchanges state information and fluxes (Landrum et al., 2013).

The CCSM4 (LM) simulation reproduces a variety of large scale climate patterns suggested by historical and proxy-data records, with Northern Hemisphere (NH) and Southern Hemisphere (SH) surface temperatures cooling to the early 1800s Common Era by 0.5 $^{\circ}$C (NH) and 0.3°C (SH), followed by warming up to present day. High latitudes of both hemispheres show polar amplification of the cooling from the Medieval Climate Anomaly (MCA) to the Little Ice Age (LIA) associated with sea ice increases. The LM simulation does not reproduce cooling contributed by La Ninã in the eastern Pacific Ocean during the MCA relative to the LIA, as has been suggested by proxy reconstructions. The Atlantic multidecadal oscillation (AMO) has higher variance at centennial periods in the (LM) simulation compared to the 1850 no transient run, suggesting a long-term Atlantic Ocean response to natural forcings. The North Atlantic Oscillation (NAO), Pacific decadal oscillation (PDO), and El Niño–Southern Oscillation (ENSO) variability modes show little or no change. CCSM4 does not simulate a persistent positive NAO or a prolonged period of negative PDO during the MCA, as suggested by proxy reconstructions (Landrum et al., 2013).

The MPI-ESM-P model consists of the atmospheric model ECHAM6 with horizontal resolution 1.87° x 1.85° providing data for the area over the Mediterranean of 160 km longitude x 200 km latitude and 47 vertical levels. Additionally, the model is coupled with the ocean model MPI-OM (bi-polar curvilinear grid: 1.5° horizontal resolution with 40 levels) (Xoplaki et al., 2015).The vegetation model JSBACH is also included, to take into account changes in land use. The model and experiment setup (Figure 3.7) are discussed in greater detail in (Giorgetta et al., 2013).

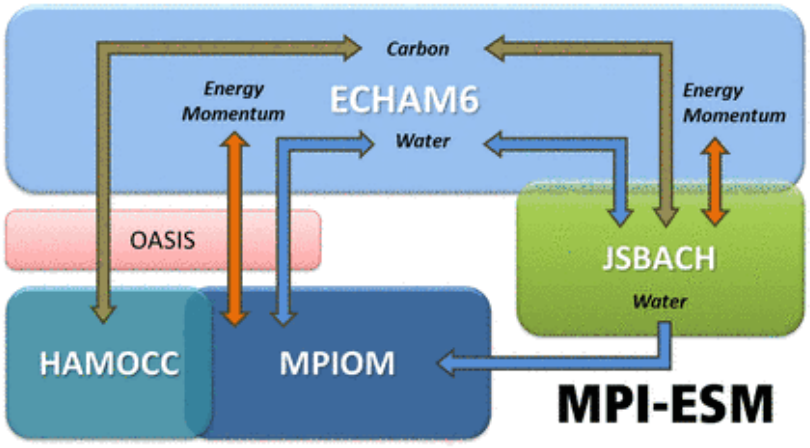

Figure 3.7: Schematic view of MPI-ESM: Colored boxes show the model components: the atmospheric general circulation model ECHAM6 is directly coupled to JSBACH land model that describes physical and biogeochemical aspects of soil and vegetation. MPIOM is the ocean general circulation model, which includes the HAMOCC model for marine biogeochemistry. OASIS is the coupler program, which aggregates, interpolates, and exchanges fluxes (for water, energy, momentum, and CO2) and state variables once a day between the aforementioned models (Giorgetta et al., 2013).

The reconstructed SST data from multicore M2 were estimated with a smoothing local adaptive kernel regression (Gogou et al., 2016) and were filtered with 100 years filter in order to provide information for the long-term behavior. Data were calculated on an annual and seasonal resolution from the average prices of the grid points given. Data anomalies were calculated with respect to the reference period 1500-1850 AD because the comparison of simulations and reconstructions is less sensitive to errors in anthropogenic aerosol forcing applied to the models when a pre-industrial reference period is used, and less sensitive to different realisations of internal variability with a multi-century reference period (IPCC, 2013). Model atmospheric data were also filtered with 100 years running mean. In order to evaluate the trends all data were calculated under a local regression smoothing.

4 RESULTS

4.1 Proxy data

4.1.1 Alkenone-based Sea Surface Temperatures (SSTs)

The Sea Surface Temperature (SST) in the multicore M2 is shown in Figure 4.1 (data from Gogou et al., 2016). The temperature values show an increase from 850 to 950 AD and from 1100 to 1300 AD with a prominent temperature peak at ~ 1600 AD. A cooling phase of almost 1.5 ºC is observed from 1600 AD to 1700 AD. After that a continuous SST warming trend is recorded, interrupted by two prominent cooling events at 1832 AD (16.6 ºC) and 1995 AD (19.1 ºC).

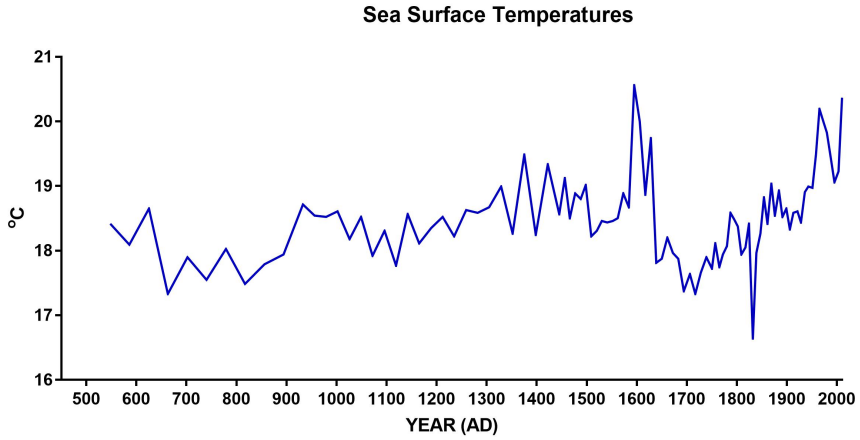

Figure 4.1: Sea Surface Temperatures (SSTs) based on alkenones in the multicore M2 (from Gogou et al., 2016).

The SST in the multicore M3 (interval between ~600- 1655 BC) is shown in Figure 4.2. The temperature values vary between 17.2 ºC (934 BC) and 22.5 ºC (688 BC). From 1655 BC till 1465 BC the SST is approximately 19 ºC. In 1465 BC the SST is a 21.4 ºC and after that there is a continuous stable SST trend of temperatures ~18 ºC until 1010 BC. A prominent cooling event (~17 ºC) occurs at 934 BC. In a period of 24 years from 934 BC to 910 BC the SSTs show an increase of 1.1 ºC. A cooling phase is observed in 839 BC but yet conditions are warmer than in 934 BC. After that and till ~600 BC a continuous SST warming trend is recorded with values exceeding 20 ºC.

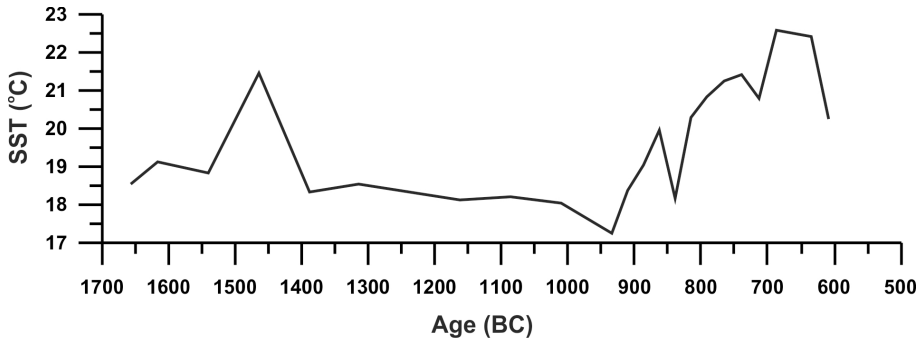

Figure 4.2: Sea Surface Temperatures (SSTs) based on alkenones in the multicore M3.

4.1.2 Isotope analyses ($\delta^{13}C$ and $\delta^{18}O$)

The stable isotopic ($\delta^{13}C$ and $\delta^{18}O$) records of the species *Globigerinoides ruber* (white) in the multicore M2 are shown in Figure 4.3. The $\delta^{18}O$ values range (Figure 4.3) from -0.67 ‰ at the end of 18th century to 1.07 ‰ at 1990 AD, with an average of 0.32 ‰. A progressive decrease between 700 AD and 1000 AD (minimum value 0.19 ‰ at 980 AD) is followed by a rapid increase (1.01 ‰) around 1150 AD.

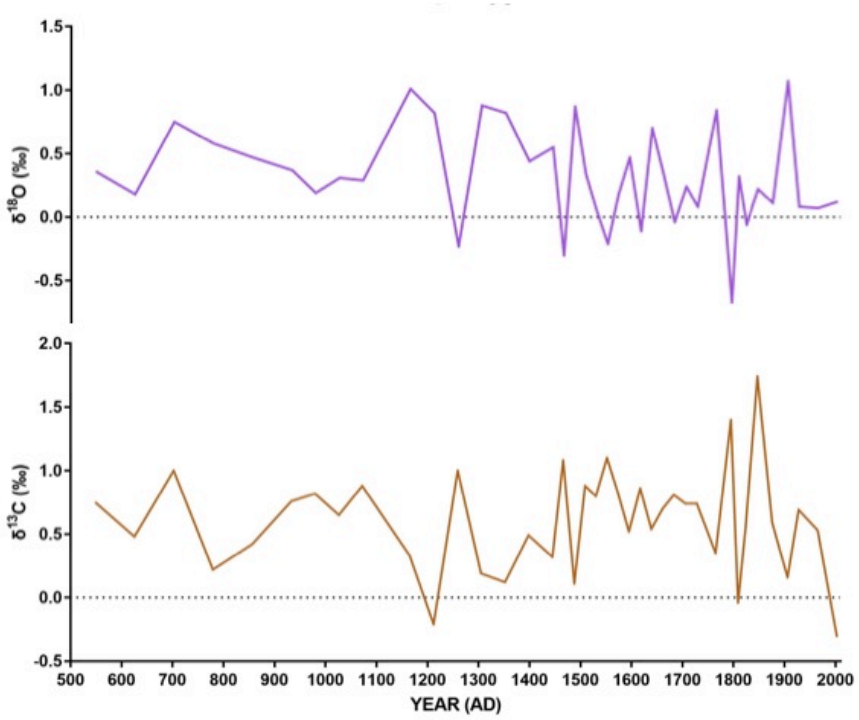

Figure 4.3: Stable isotope ($\delta^{13}C$ and $\delta^{18}O$) records of the species *Globigerinoides ruber* (white) in the multicore M2.

Between 1150 AD and 1500 AD, $\delta^{18}O$ remained to heavier values, with two abrupt drops at 1260 AD (-0.23 ‰) and 1470 AD (-0.30 ‰). Afterwards and until present the record is characterized by significant fluctuations and mainly low values; significantly high values are observed around 1640 AD (0.70 ‰), 1760 AD (0.84 ‰) and 1900 AD (1.07 ‰).

The $\delta^{13}C$ values (Figure 4.3) range from -0.31 ‰ at 2000 AD to 1.74 ‰ at 1850 AD, with an average of 0.60 ‰. The general trends exhibit a relative opposite pattern in respect to $\delta^{18}O$ curve. The $\delta^{13}C$ shows relative high values (up to 1.00 ‰) until around 1100 AD, and low values (max=0.49 ‰) between 1150 AD and 1450 AD, with two prominent increases at 1260 AD (1.00 ‰) and 1470 AD (1.08 ‰). After that a relatively constant pattern is observed, with an average value of 0.77 ‰, until 1730 AD. During the last 250 years, the record is characterized by large fluctuations; notable high values around 1800 AD (1.40 ‰), and 1850 AD (1.74 ‰) are alternated with significantly low values at 1810 AD (-0.04 ‰), 1900 AD (0.16 ‰) and 2000 AD (-0.31‰).

4.1.3 Benthic foraminifera - Low Oxygen (LO) index

The abundance of low oxygen indicators (LO) in the multicore M2 is shown in Figure 4.4. The LO values shows relatively low values and varies between 4 % (1730 AD) and 27 % (2000 AD), with an average of 14 %. Until 1100 AD, relative high values (up to 23%) are observed, except for the time interval between 800 AD and 850 AD, where a rather abrupt decrease (down to 7 %) occurs. Between 1150 AD and 1730 AD, the record is characterized by constantly low values, with an average of 11 %. A significant peak (21 %) in LO index is detected around 1740 AD. During the last 200 years, the LO values display a progressively increasing trend (max= 27 % at 2000 AD).

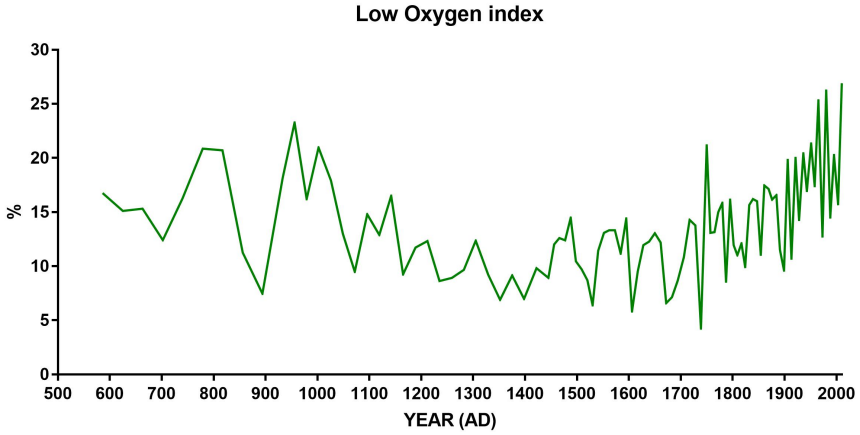

Figure 4.4: Low oxygen (LO) index in the multicore M2.

4.1.4 Coccolithophores - Stratification S index

The S index in the multicore M2 is shown in Figure 4.5. The S index values vary between 0.11 (625 AD) and 0.69 (1600 AD), with an average of 0.35. Main positive shifts in the water column stratification occur between 1450 AD and 1600 AD (up to S=0.66) and between 1700 AD and 1750 AD (up to 0.60). After that, relative low values (down to 0.15 at 1780 AD) for the index are recorded. At the beginning of the 19th

century, the S index presents a progressive increase, with maximum value 0.60 at 1950 AD.

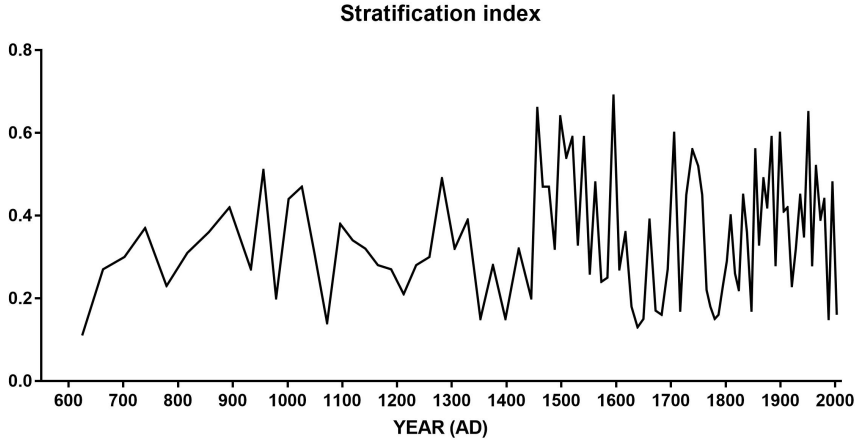

Figure 4.5: Stratification (S) index in the multicore M2.

4.2 SST based on alkenones reconstruction and CMIP5 simulations

4.2.1 Annual and Winter Precipitation analysis - Aegean SST

In this study, we compare the annual precipitation anomalies, as given from different model simulations (CCSM4 r1, MPI-ESM-P r1 and MPI-ESM-P p2k) over the last two millennia with the estimated alkenone temperature proxy in the northern Aegean (NE Mediterranean) during the last 1500 years (Figure 4.6). During the RWP, simulated data of MPI-ESM-P p2k model show positive anomalies. However, a significant decreasing trend occurs from the middle 2nd century and negative anomalies follow until the end of the 5th century (DA). Another rather abrupt decrease in simulated precipitation anomalies is observed between ~550 AD and ~650 AD (LALIA).

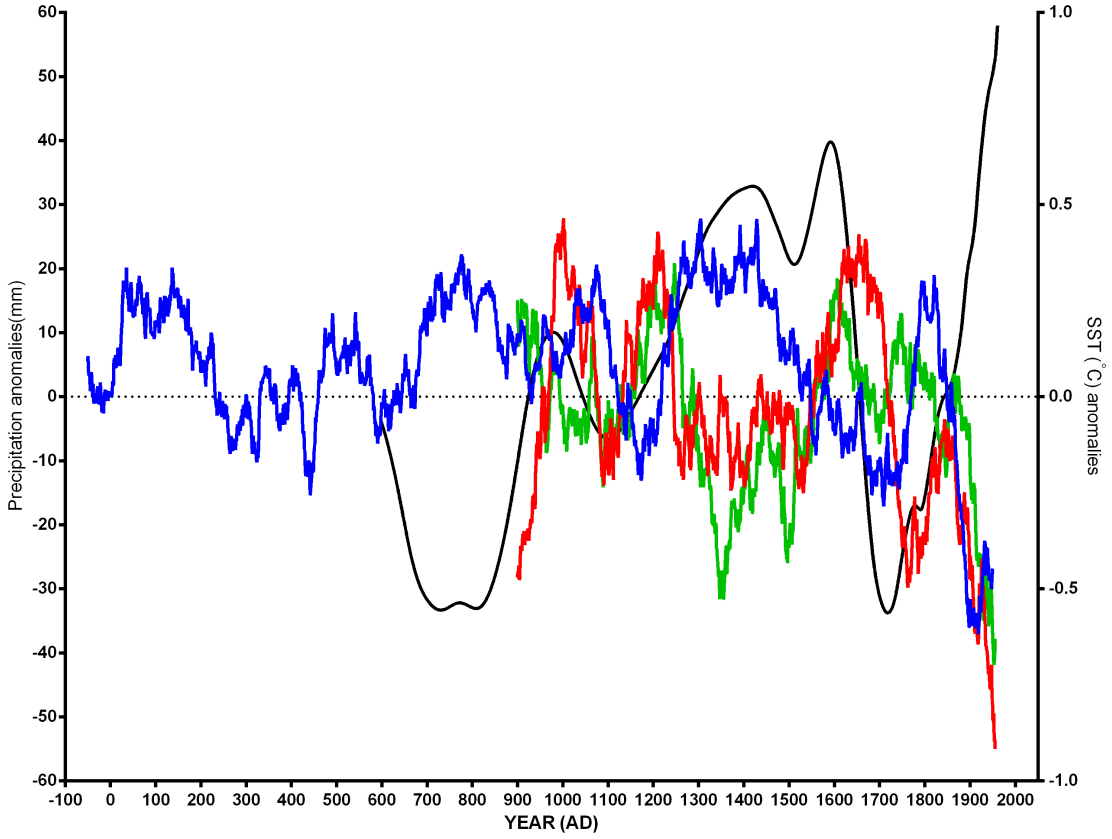

Figure 4.6: Annual Precipitation anomalies (wrt 1500-1850) for different model simulations and comparison with Aegean SST based on alkenones reconstruction. MPI-ESM-P p2k (blue); MPI-ESP-P r1 (red); CCSM4 r1 (green); SST (black).

During the MCA, MPI-ESP-P r1 and MPI-ESM-P p2k precipitation simulations show mostly positive anomalies, exhibiting wet climate conditions, whereas the CCSM4 r1 model presents an opposite trend, with negative anomalies from the end of 10th until 1250 AD (Figure 4.6). Significant disagreement between models exists during the LIA, where MPI-ESP-P r1 and CCSM4 r1 simulations with high negative anomalies displaying dry climate conditions, whereas r1MPI-ESM-P p2k shows wet conditions (~1200 to ~1550 AD). Until 1850 AD, simulated data present high variability. After 1850 AD, all model simulations exhibit a similar sharp drier trend.

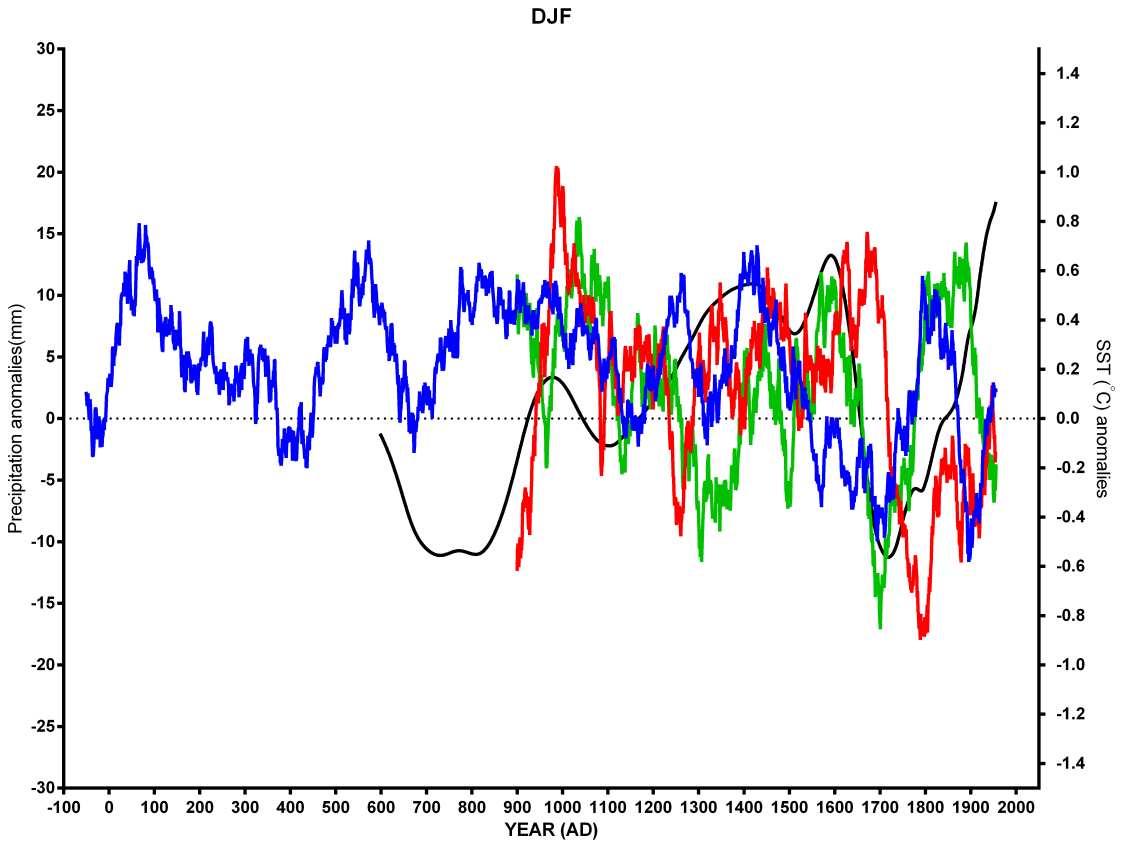

Figure 4.7: Winter Precipitation anomalies (wrt 1500-1850) for different model simulations and comparison with Aegean SST based on alkenones reconstruction. MPI-ESM-P p2k (blue); MPI-ESP-P r1 (red); CCSM4 r1 (green); SST (black).

The winter precipitation anomalies (Figure 4.7) show a slightly smaller variability than the annual simulated data. During the MCA, all three model simulations present generally improved agreement than annual precipitation anomalies; however, disagreement still exists over the LIA.

4.2.2 Annual Temperature Analysis-Aegean SST

For the time periods between the Roman Warm Period (RWP, before 300 AD) and the Late Antique Little Ice Age (LALIA, 536-around 660 AD: (Büntgen et al., 2016); (Toohey et al., 2016) only simulated data by the MPI-ESM-P p2k model are available. In general, simulated SSTs show positive anomalies, exhibiting warm conditions (Figure 4.8). However, a significant decreasing trend of temperature occurs during the first 300

years, and then a marked increase follows until the end of the RWP (Figure 4.9a). During the Dark Ages (DA, ~300-600 AD) time period, a significant peak in simulated SST anomalies is detected in the middle of 5th century (Figure 4.9b). A rather abrupt decrease, between 550 AD and 600 AD (LALIA) is observed (Figure 4.9c).

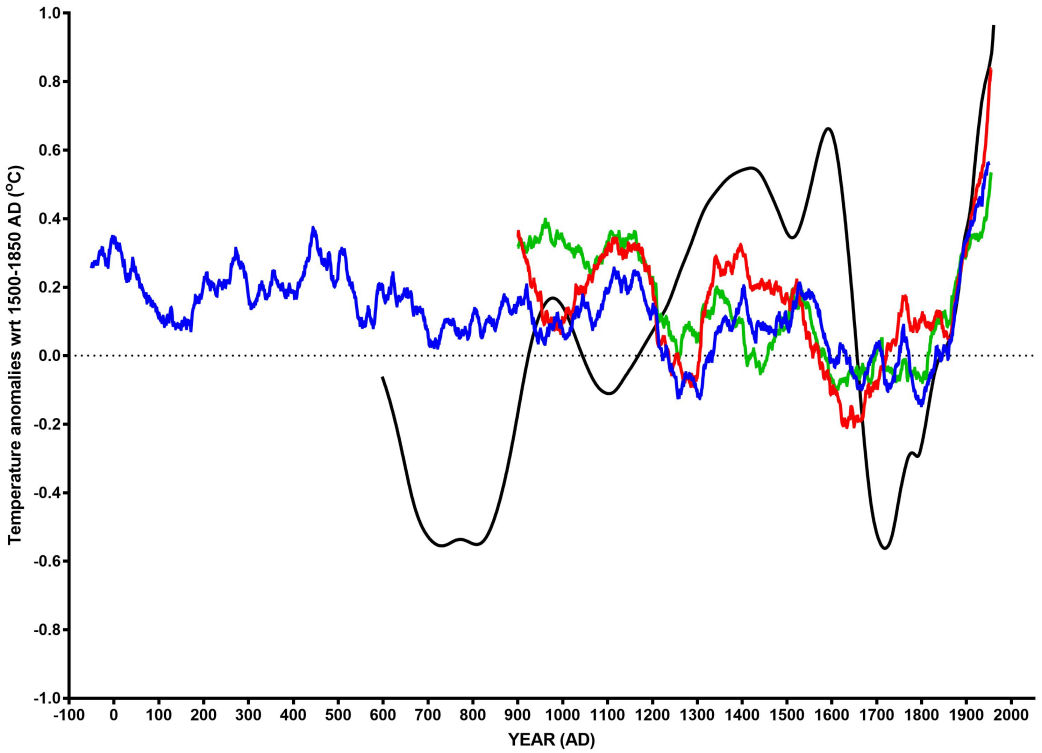

Figure 4.8: Annual Temperature anomalies (wrt 1500-1850 AD) for different model simulations and comparison with Aegean SST based on alkenones reconstruction. MPI-ESM-P p2k (blue); MPI-ESP-P r1 (red); CCSM4 r1 (green); SST based on alkenones reconstruction (black).

After 850 AD, all three model simulations present generally similar evolution in annual temperatures anomalies. Disagreement between models exists in the time interval of 910-1065 AD, where CCSM4 r1 simulation shows an opposite pattern and warmer conditions than MPI-ESP-P r1 and MPI-ESM-P p2k. Nevertheless, during the Medieval Climate Anomaly (MCA ~600-1200 AD) and especially within the 13th century, all simulations show large warm biases (Figure 4.9d). During the 2nd half of the 14th century and later from the middle 16th until early 18th century (1570-1720 AD), all three model simulations show two cold signals, corresponding to the Little Ice Age (LIA, ~1200-1850 AD) period

(Figure 4.9e). In beginning the 18th century, SST anomalies of MPI-ESP-P r1 show a trend toward more positive values, in contrast of those observed in CCSM4 r1 and MPI-ESM-P p2k. After 1850 AD, all model simulations present a similar sharp warm trend (Figure 4.9f).

The SST time series shows a cold period during the 7th until the early 10th century. The period from the 10th until the middle 11th (MCA) is characterized by warmer conditions. From the middle of 11th until the end of the 12th century (1170 AD) northern Mediterranean SSTs show again cooler conditions. After this there is a long period until the middle 17th century with generally above normal SSTs.

From the 2nd half of the 17th century there is a strong cooling of approx. 1°C within a few years. Until the mid 19th century SSTs are below the 1500-1850 climatology, followed by a strong warmer trend. Except for the last 150 years, there is no agreement between the SST record and the paleo model simulations. The SST record clearly shows stronger amplitudes.

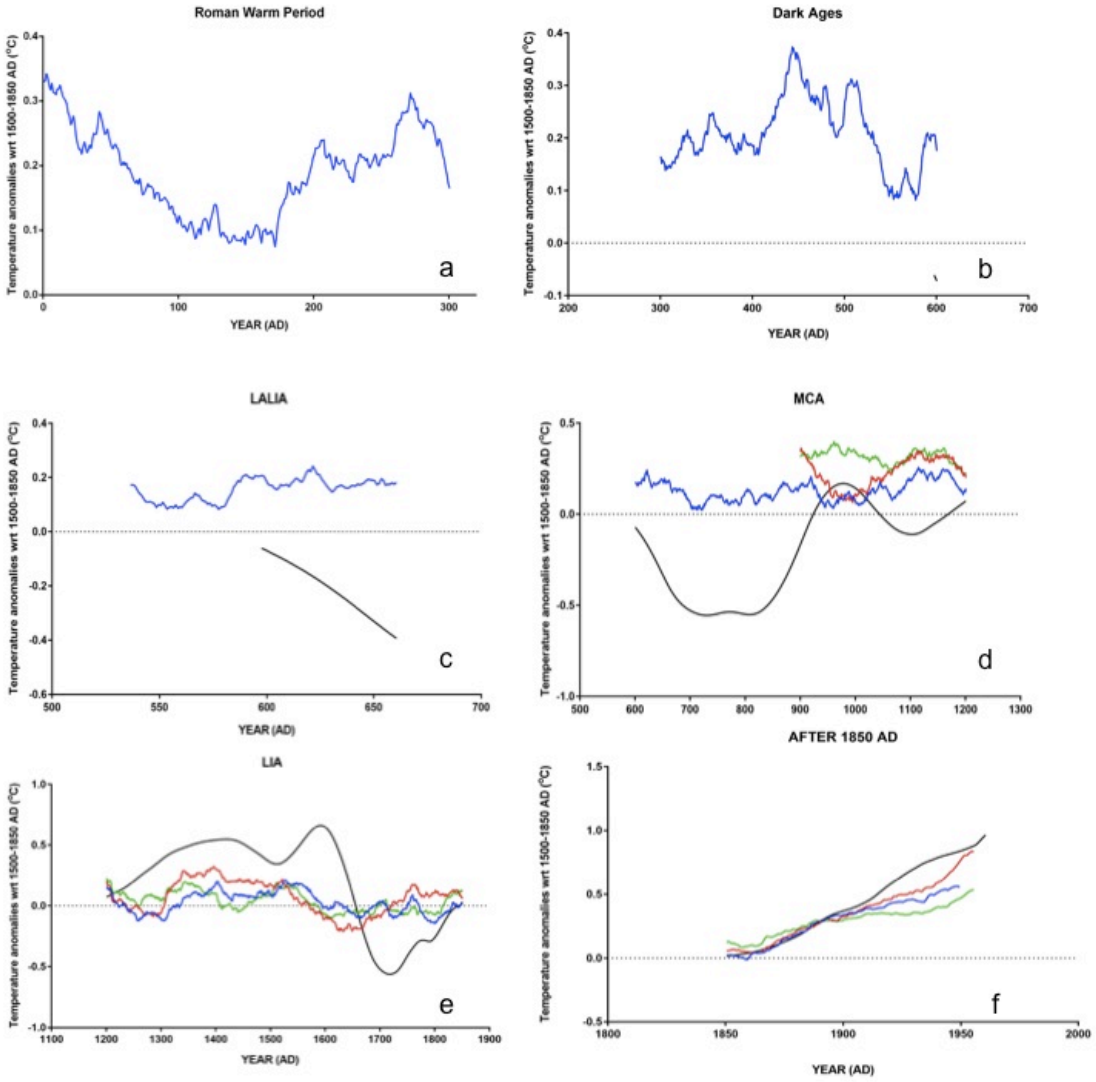

Figure 4.9: Annual Temperature anomalies (wrt 1500-1850 AD) for different model simulations and comparison with Aegean SST based on alkenones reconstruction: a. Roman Warm Period for the Aegean Region, b. Dark Ages, c. Late Antique Little Ice Age, d. Medieval Climate Anomaly period, e. Little Ice Age period, f. after 1850 AD period. MPI-ESM-P p2k (blue); MPI-ESP-P r1 (red); CCSM4 r1 (green); SST based on alkenones reconstruction (black).

5 DISCUSSION

The multidisciplinary approach applied in this Thesis uses selected micropaleontological evidence and marine indices retrieved from the M2 and M3 sedimentary records in combination with paleo model simulations. This research focuses on reconstructing past climatic changes of the North Aegean, due to its unique physical and geographic characteristics.

5.1 Climate variability of the North Aegean region based on M2 proxy reconstructions

5.1.1 Bronze Age (BA) - Iron Age (IA) ~2000–586 BC

Dry conditions are dominant during this period for the western Mediterranean and are associated with Saharan eolian input fluctuations (Nieto-Moreno et al., 2011). This aridification trend coincides with a progressive evolution towards typical Mediterranean climate and aridity, which gradually occurs from the middle Holocene and with one of the major periods of Holocene rapid climate change (RCC) at ~3500– 2500 cal yr BP (Mayewski et al., 2004). The Sea Surface Temperatures in the North Aegean Sea are between 22.5 ºC (688 BC) and 17.2 ºC (934 BC) (Figure 5.1). The 934 BC is in the middle of the duration of the RCC.

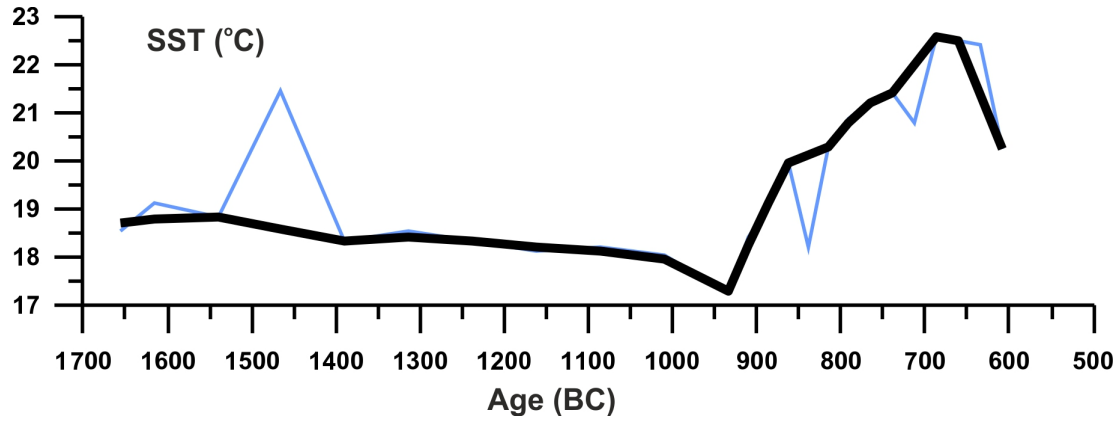

Figure 5.1: Core M3: Sea Surface Temperature (SST), Thin curves indicate row data and thick ones a local regression smoothing.

During these RCC periods a higher intensity of dust export and wind speeds have been described, which may explain the low latitude aridity associated with this period along with a decline in the Northern Hemisphere solar insolation (Steinhilber et al., 2009). The prevailing paleoceanographic conditions during this period entail faster flowing and better oxygenated bottom waters, low productivity and, owing to better oxygenated bottom sediments, lower organic matter preservation (Nieto-Moreno et al., 2011). From 1655 BC till 950 BC the SSTs have a cooling trend. In a period of 24 years from 934 BC to 910 BC the SST show an increase of 1.1 ºC. Until 650 BC there is a continuous warm trend. After that a continuous SST warming trend is recorded of SSTs above 20.2 ºC, which can be correlated with reduced water column mixing (Kouli et al., 2012). The beginning of the Middle Bronze Age-Iron Age period is marked in the central Mediterranean Sea by a dominance of planktonic foraminifera suggesting oligotrophic conditions, high productivity surface waters, strong seasonality and the presence of continental runoff (Margaritelli et al., 2016).

5.1.2 Medieval Climate Anomaly (MCA) 600 to 1200 AD

In the northern Aegean, proxy-reconstructions of the M2 record reveal an SST cooling trend of almost 1ºC from 500 to 850 AD followed by a warming trend from 850 AD to 950 AD (Figure 5.2; alkenone SST data from Gogou et al., 2016). Based on the current knowledge for the Mediterranean region, the first six centuries AD included some of the most intense and long- lasting droughts of the late Holocene in the Middle Eastern region (Roberts et al., 2012). A progressive decrease of $\delta^{18}O$ values between 700 AD and 1000 AD is followed by a rapid increase around 1150 AD (Figure 5.2). During the same period there is high supply from continental/riverine runoffs and elevated in-situ productivity which support the hypothesis of enhanced continental inputs (Gogou et al., 2016). $\delta^{13}C$ measurements show how much of the seasonal fluctuations is controlled by the terrestrial biosphere versus oceanic exchange (e.g., Gogou et al., 2007). The M2 $\delta^{13}C$ shows relative high values until around 1100 AD. Until 1100 AD the increase of LO-index implies low-oxygen bottom conditions (e.g., Kuhnt et al., 2007); (Triantaphyllou et al.,

2016) in contrast the time interval between 800 AD and 850 AD displays a rather abrupt LO-index decrease (Figure 5.2).

High values in the S-index generally indicate relatively deep nutricline/thermocline position and intensified stratification conditions in the water column, while low values imply high surface waters paleoproductivity (Flores et al., 2000). From 850 to 950 AD there is higher preservation of organic matter due to reduced water column mixing (Kouli et al., 2012). In line, the Stratification index (S) has a rising trend during the same period indicating stratified water column that favored preservation in bottom waters; its lowest values are at 950AD and 1100 AD, pointing to intense water column mixing. Periods of rather high stratification in the north Aegean Sea are well correlated with findings from previous studies, highlighting major flood events in the eastern Mediterranean (Luterbacher et al., 2012); the presence of fresh water lid triggering stratified conditions in the water column (e.g., Gogou et al., 2016); Triantaphyllou et al., 2016).

5.1.3 Little Ice Age (LIA) 1200 AD to 1850 AD

A cooling phase of almost 1.5 ºC is observed from 1600 AD to 1700 AD. During this period stratification index decreases and productivity increases (Figure 5.2) probably due to enhanced winter mixing conditions (Gogou et al., 2016). A continuous SST warming trend is following, interrupted by a prominent cooling event at 1832 AD (16.6 ºC) (Figure 5.2). According to Gogou et al. (2016), this event is possibly related to an 'unknown' volcano eruption in 1809 and the April 1815 Tambora volcanic eruption (Oppenheimer, 2003). High-resolution paleolimnological data from the Iberian peninsula show good inter-site coherence and indicate lower water levels and higher salinities synchronous with the MCA and generally more humid conditions during the LIA (Roberts et al., 2012). This pattern is in agreement with other lake, marine and tree ring records from Iberia and Morocco (Esper et al., 2007). Lake and partly speleothem evidence from Turkey shows an opposite pattern of a wet MCA and a dry LIA (Roberts et al., 2012). Warm coccolithophore species increase between 1550-1700 AD, support high surface water temperatures, whereas rise in the S-index between 1450-1600 AD points to the

development of Deep Chlorophyll Maximum (DCM) and intensification of the water column stratification that likely promotes in-situ preservation of exported organic matter (Gogou et al., 2016).

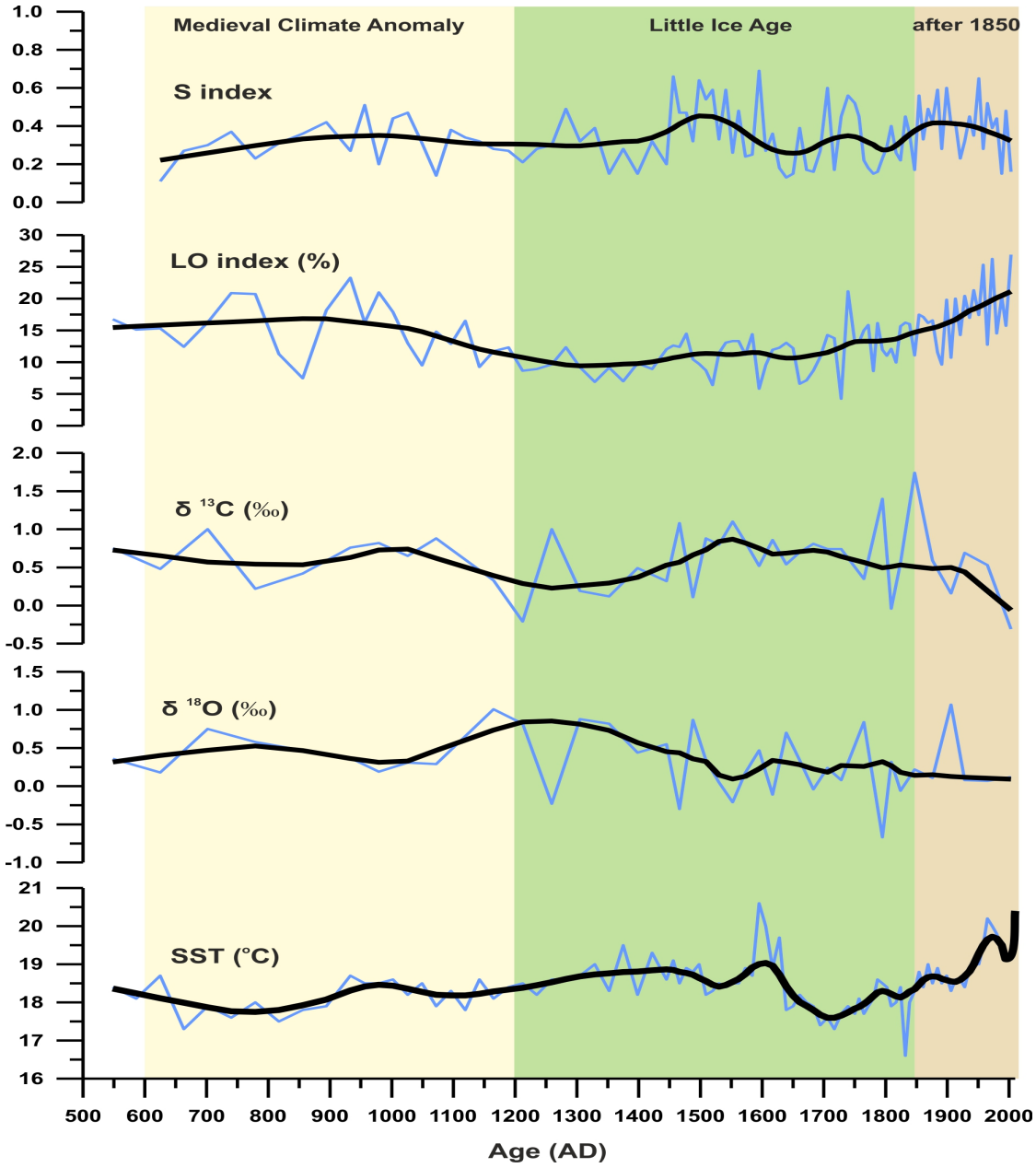

Figure 5.2: Core M2: Sea Surface Temperature (SST), $\delta^{18}O$, $\delta^{13}C$, Low Oxygen (LO) index, Stratification (S) index for Medieval Climate Anomaly, Little Ice Age and after 1850 AD. Thin curves indicate row data and thick ones a local regression smoothing.

From 1000 to 1300 AD there is an establishment of low-salinity stratified waters and the presence of nutrient-rich environment in the deep photic zone (Gogou et al., 2016). The north Aegean M2 record shows recent warming initially starting after 1100 AD and intensified after 1700 AD, which is also recorded in the core from the Gulf of Taranto (Grauel et al., 2013b) and in an Alboran sea core (Nieto-Moreno et al., 2013). The $\delta^{18}O$ remained to heavier values between 1150 AD and 1500 AD, with two abrupt drops at 1260 AD and 1470 AD. After that there are significant fluctuations and mainly low values until around 1640 AD when significantly high values are observed. The general trends of $\delta^{13}C$ exhibit a relative opposite pattern in respect to $\delta^{18}O$ curve (Figure 5.2). Greater values of $\delta^{18}O$ reflect cold climate, while lower ones indicate warm climatic conditions (Waelbroeck et al., 2005 ; Emeis et al., 2000; Emeis et al., 1998 ; Rohling and Cooke, 1999; Rohling, 2007). The distribution of oxygen isotopes is primarily controlled by precipitation-evaporation and is also affected by the mixing of different water masses (Waelbroeck et al., 2005). During the middle of 13^{th}, 15^{th}, 16^{th} century the dominant conditions as reflected by the isotopical analysis are warm and match with the alkenone SST measurements (Figure 5.2). According to Xoplaki et al.(2015) cooler and more arid conditions are visible in lake palaeoclimate records during the middle of 13^{th} century and the models capture a significant decline in temperature connected with the volcanic eruption of Samalas around 1257AD. A 2200-year-long record based on foraminiferal $\delta^{18}O$ has been obtained by Taricco et al. (2009) along the Gulf of Taranto in the Central Mediterranean Sea. The record reveals a minimum in $\delta^{18}O$ at 1000AD and a maximum within LIA (1600–1800 AD), followed by a steep variation since the beginning of the Industrial Era (Figure 5.2). Multiproxy records derived from sediments of the southeastern Mediterranean Sea (Schilman et al., 2001) and the Adriatic Sea (Piva et al., 2008b) reveal complex paleo-oceanographic changes during the late Holocene, with anomalies during the Medieval Warm Period (1150 AD) and the LIA (1730 AD).

The $\delta^{13}C$ shows relative low values between 1150 AD and 1450 AD, with two prominent peaks at 1260 AD and 1470 AD (Figure 5.2). After that a relatively constant pattern towards heavier values is observed, with an average value of 0.77 ‰, until 1730 AD. During the first half of the 18^{th} century (Sisma-Ventura et al., 2009) suggested that the

eastern basin cooled by 1°C more than the western basin. $\delta^{13}C$ signal, as a proxy for primary productivity of the surface water, was enriched in nutrient levels during this coldest LIA period, due to increased vertical mixing and upwelling, which fits well with our increased $\delta^{13}C$ values that reflect increased productivity probably associated with vertical mixing. The oxygen isotope records of radiocarbon-dated samples suggest that during the LIA maximum the seawater temperature was about 2°C and 3°C colder than the present day in the western and the eastern Mediterranean basins, respectively (Sisma-Ventura et al., 2009). Between 1150 AD and 1730 AD, the record of LO is characterized by constantly low values indicating dysoxic conditions. A significant peak in LO index is detected around 1740 AD, indicating dysoxic conditions.

5.1.4 Industrial period: after 1850 AD

The Sea Surface Temperature has a continuous SST warming trend, interrupted by two prominent cooling events at 1832 AD (16.6 ºC) and 1995 AD (19.1 ºC). The $\delta^{18}O$ values range with an average of 0.32 ‰, displaying a minimum of -0.67 ‰ at the end of 18th century indicating warm surface water conditions and a maximum of 1.07 ‰ at 1900 AD which suggest an abrupt cold climatic event. The Industrial Period is overall characterized by an increase of warm water planktonic foraminiferal species also in the central part of the Mediterranean (Margaritelli et al., 2016). Until present the $\delta^{18}O$ record is characterized by significant fluctuations and mainly low values; significantly high values are observed around 1760 AD and 1900 AD. The $\delta^{13}C$ values range from -0.31 ‰ at 2000 AD to 1.74 ‰ at 1850 AD, with an average of 0.60 ‰. High values imply an increase in marine productivity. In the second part of the 17th century and early 18th century, stratification of the upper water column decreases with concomitant productivity increase, as witnessed by lowering of the S-index and $d^{13}C$ values, due probably to enhanced winter mixing conditions (Gogou et al., 2016). At the beginning of the 19th century, the S index presents a progressive increase, with maximum value 0.60 at 1900 AD. During the last 250 years, the record is characterized by large fluctuations; notable

high values around 1800 AD, and 1850 AD are alternated with significantly low values at 1810 AD and 1900 AD. The LO values shows relatively low values from 1730 AD to 2000 AD with an average of 14 %. During the last 200 years, the LO values display a progressively increasing trend, maximum at 2000 AD which follows the increasing trend in SSTs (Figure 5.2) and reflect the global generally warming trend of the Industrial Period.

5.2 North Aegean climate variability based on the paleo-climate model reconstructions

5.2.1 Annual and Seasonal Precipitation analysis - correlation with Aegean SST

Precipitation is a complex process in the Mediterranean region and this is why in this thesis the results from the model – SST comparison are not entirely indicative for this region since the alkenone SST provides information for a specific small domain size in contrast to the wider area of data from the models. The more regional character of the analysis is the more impact the initial conditions of all climate subsystems to start the simulation might have on the years immediately following. The complex topography of the region and the complex processes affect precipitation. The correlation between Aegean SST and the annual as well as seasonal precipitation simulations are unclear and most often non-significant (Figure 5.3).

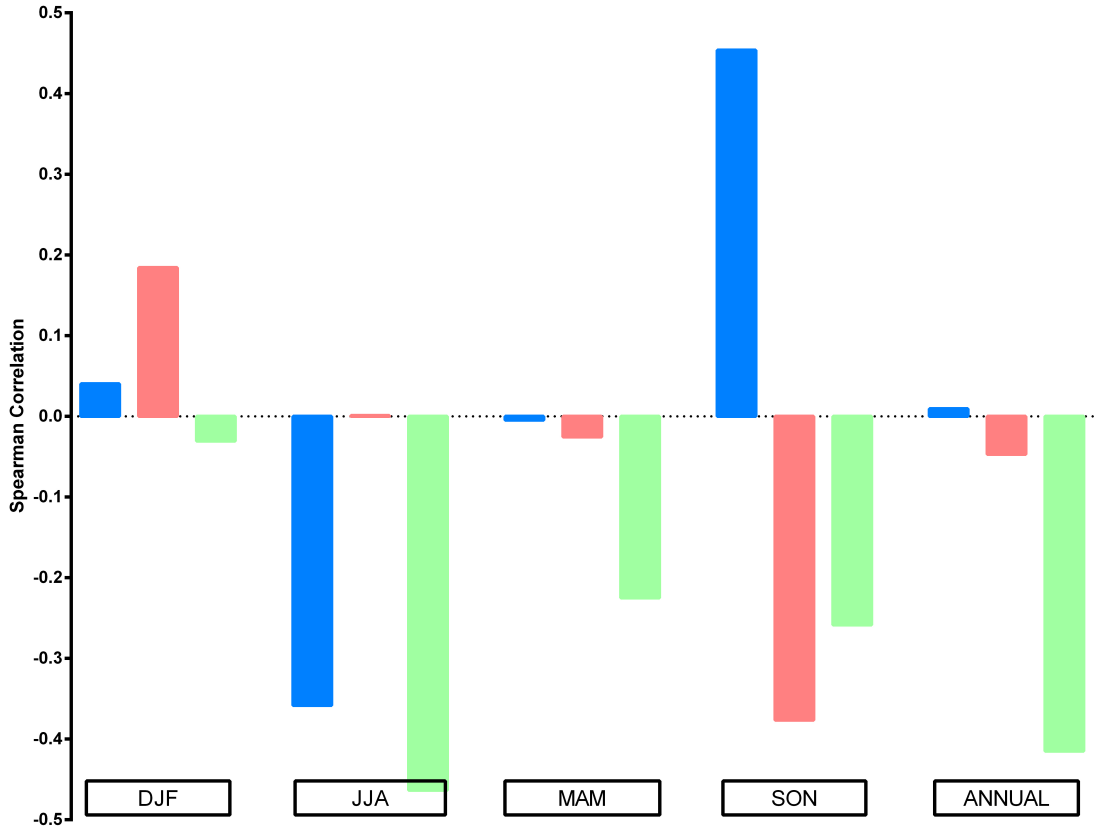

Figure 5.3: Spearman's rank correlation coefficient (r) between paleo climate models and Aegean SST for annual and seasonal analysis. DJF (winter, December to February); JJA (summer, June to August); MAM (spring, March to May); SON (autumn, September to November). MPI-ESM-P p2k (blue); MPI-ESP-P r1 (red); CCSM4 r1 (green).

5.2.2 Annual and Seasonal Temperature Analysis - correlation with Aegean SST

Alkenones are synthesized by algal species of the Prymnesiophyte class e.g., *Emiliania huxleyi*, a species that prevails within the mixed layer in the Aegean during the winter and early spring season. A recent sediment trap study in the Northern Aegean Sea has shown that *E. huxleyi* coccoliths dominate in the total coccolith flux on an annual basis, however the higher production and export rates is occurring between February and June (Triantaphyllou et al., 2014). In this study, the Pearson's correlation coefficients (Figure 5.4) were calculated to investigate the agreement between Aegean SST based on alkenones reconstruction and the seasonal as well as the annual simulated trends.

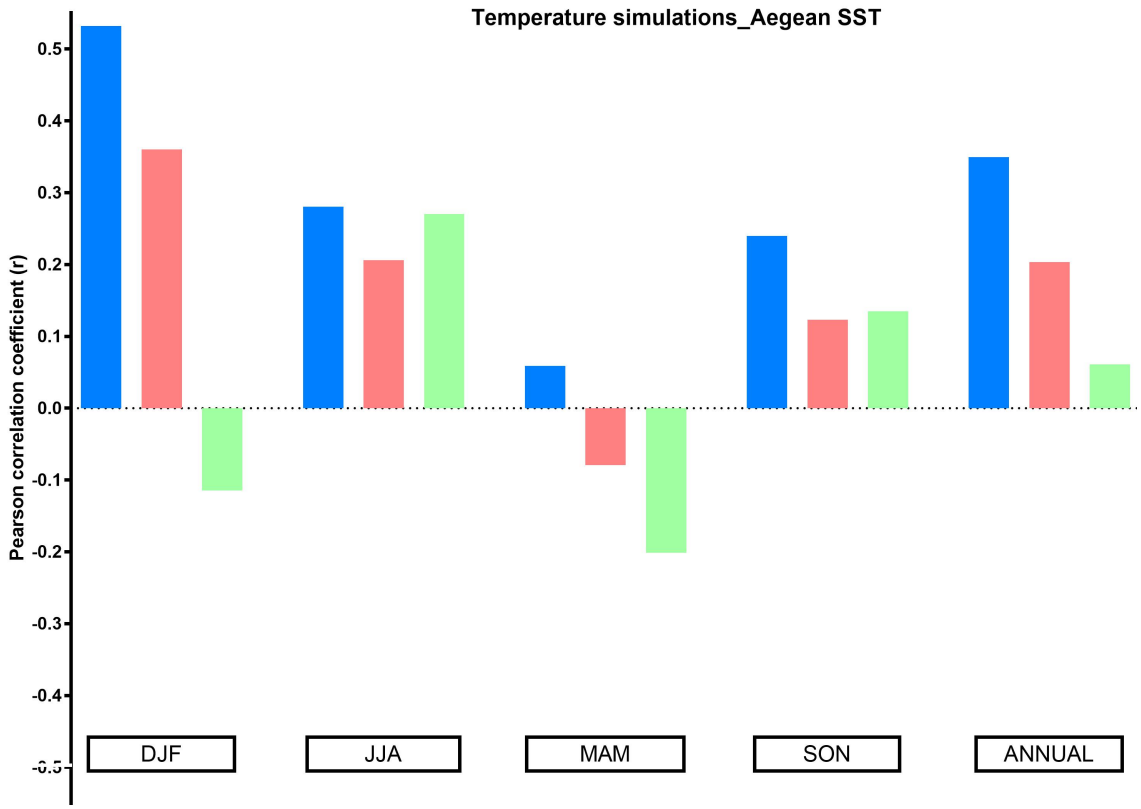

Figure 5.4: Pearson correlation coefficients (r) between paleo climate models and Aegean SST for annual and seasonal analysis. DJF (winter, December to February); JJA (summer, June to August); MAM (spring, March to May); SON (autumn, September to November). MPI-ESM-P p2k (blue); MPI-ESP-P r1 (red); CCSM4 r1 (green).

The analysis (Figure 5.4) shows significant positive correlations for the annual simulations: CCSM4 r1 ($r = 0.06$, $p < 0.05$), MPI-ESM-P r1 ($r = 0.20$, $p < 0.05$) and MPI-ESM-P p2k ($r = 0.35$, $p < 0.05$). However, MPI-ESM-P p2k exhibits better agreement with Aegean SST. Highly significant positive correlations are shown for winter (Figure 5.4,Figure 5.5) in MPI-ESM-P r1 and MPI-ESM-P p2k models ($r = 0.20$ and $r = 0.35$, $p < 0.05$ respectively), whereas the CCSM4 r1 model for the same season presents negative correlation ($r = -0.11$, $p < 0.05$). The correlation coefficient for the spring in CCSM4 r1 is also negative ($r = -0.20$, $p < 0.05$), but the MPI-ESM-P r1 and the MPI-ESM-P p2k simulations in this case show a non-significant correlation ($r = -0.08$ and $r = -0.06$, $p > 0.05$ respectively).

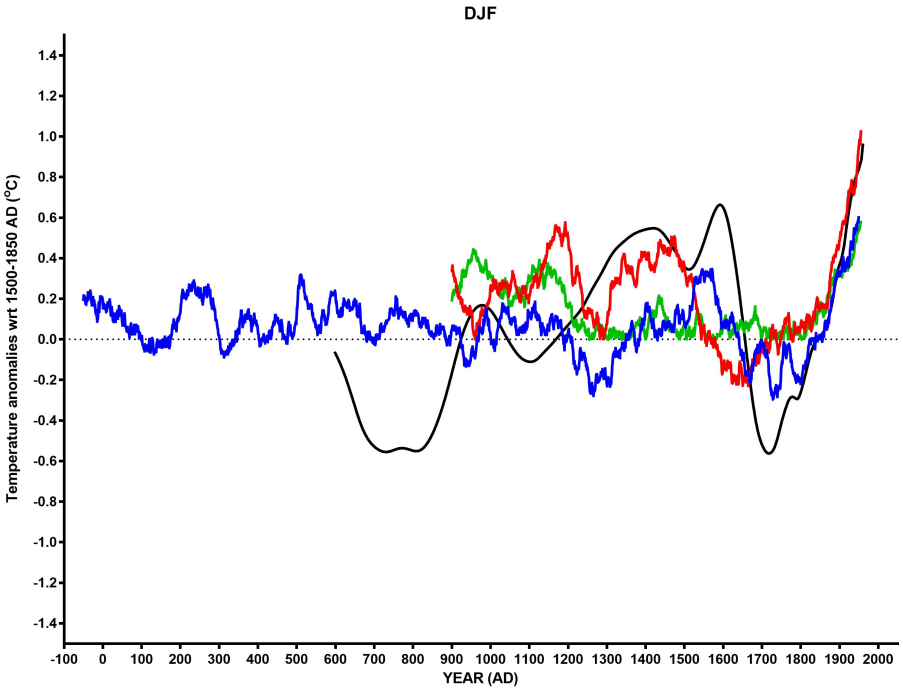

Figure 5.5: Winter Temperature anomalies (wrt 1500-1850 AD) for different model simulations and comparison with Aegean SST based on alkenones reconstruction. MPI-ESM-P p2k (blue); MPI-ESP-P r1 (red); CCSM4 r1 (green); SST based on alkenones reconstruction (black).

The running correlations (Figure 5.6) filtered with 100 years running mean show the variations in the relationships between the annual as well as winter simulations and Aegean SST. All three model simulations suffer large fluctuations over time. The maximum negative correlation observed from the middle 12th until early 13th century. The annual time series show strong positive correlations from the middle of 13th until early of the 14th century and after 1800 AD (Figure 5.6a). Throughout the winter correlation time series (Figure 5.6b), the CCSM4 rl mostly remains in negative values. These results support the annual and winter visual inspection, shown in Figure 4.8 and Figure 5.5 respectively.

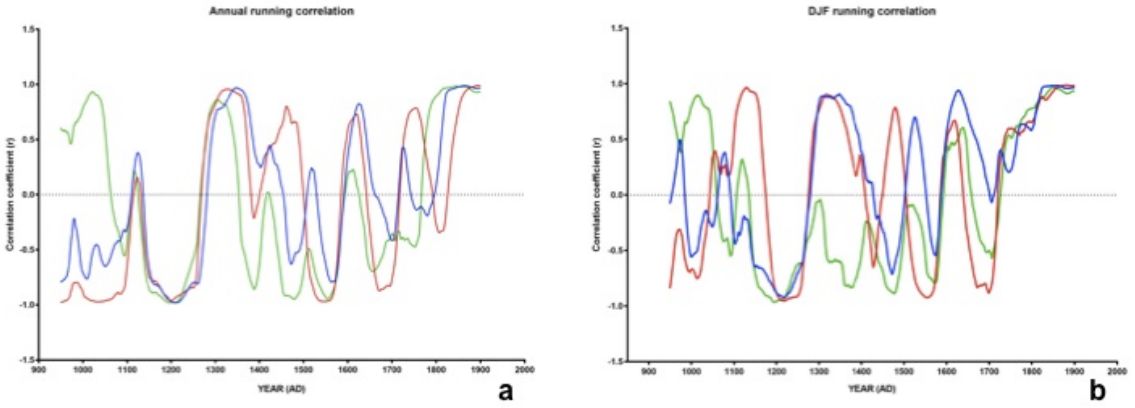

Figure 5.6: a. annual and b. winter running correlation between model simulations and Aegean SST. MPI-ESM-Pp2k (blue); MPI-ESP-P r1 (red); CCSM4 r1 (green).

The differences between the model simulations are due to different forcings, physical implementations, time trajectories and internal variability (CCSM4 r1 used the volcanic forcing data (Gao et al., 2008) and MPI-ESM-P used the volcanic reconstruction (Crowley and Unterman, 2013), CCSM4 does not simulate a persistent positive North Atlantic Oscillation (NAO) or a prolonged period of negative PDO during the MCA, as suggested by proxy reconstructions (Landrum et al., 2013). In the Mediterranean Sea, positive winter NAO is connected with relatively warm western Mediterranean and cold eastern Mediterranean Basin (Luterbacher and Xoplaki, 2003). The time trajectory of the internal climate variability is in practical terms unpredictable: since its evolution depends on all details of the state of the atmosphere, the ocean and other subsystems at a certain point in time, and this detailed knowledge is practically impossible to attain. The internal variability is higher during periods with only little changes in solar and volcanic activity. The SST is considered to be the mean annual value, through these results we can say that it mostly represents the bloom of *E. huxleyi* during February/March (Triantaphyllou et al., 2010; Triantaphyllou et al., 2004) and it is mostly affected by the winter period (Figure 5.5).

During the RWP the dominant conditions are warm with a max drop but still warm in 172 AD. The warmest conditions can be found around at the end of the 5th century. In contrast, cooler alkenone SSTs are found at the end of the 6th century and they are possibly linked to the LALIA and to the strong volcanic forcing during that time. During

the LALIA the MPI-ESM-P p2k shows warm conditions whereas the SST cools down; in this occasion either the model might be off, therefore the reconstructions are uncertain, or internal variability is more important than forced.

During the MCA all paleo model simulations show anomalous warm climatic conditions with the CCSM4 r1 to have the warmest values in reverse correlation with the rest during 910-1065 AD. During the same period the SSTs provide warm signal. From the base of M2 record until 925 AD the SSTs behave in a complete different way.

During LIA and until the mid 17th century the SST values show warm conditions which then change into cold ones until the end of the period. For the CCSM4 r1 and MPI- ESM-P, there are common signals induced by large volcanic eruptions in the thirteenth century, e.g., the Samalas volcanic eruption in 1257 AD (Lavigne et al., 2013; Sigl et al., 2015) and the Quilotoa eruption in 1275 AD, (Ledru et al., 2013; Mothes and Hall, 2008; Sigl et al., 2015). Despite their strength, the eruptions are not reflected in the second and third ensemble of the MPI-ESM-P simulations (Xoplaki et al., 2015), which might be partly related to the slight differences in the experiment setup (Jungclaus et al., 2014). The three different model simulations show mostly warm conditions throughout the specific period. For the period after 1850 AD, the three models are in agreement with the increasing trend of the reconstructed alkenone SSTs (Gogou et al., 2016).

The correlation coefficient between the annual MPI- ESM-P p2k and the SST values is the highest among the model simulations with 95% statistical significance of low pass filter. The MPI- ESM-P p2k is based on the components of ECHAM6 for atmosphere and MPIOM for ocean as well as JSBACH for terrestrial biosphere and HAMOCC for the ocean´s biogeochemistry (Bothe et al., 2013), it has an improved representation of surface albedo, new and improved representation of the aerosol. Only discriminating by the volcanic forcing, the MPI- ESM-P p2k uses the volcanic reconstruction of (Crowley and Unterman, 2013) whereas the CCSM4 used the volcanic forcing data (Gao et al., 2008). All simulations driven by the same external forcing should theoretically produce the same external climate variability. In contrast, the time trajectory of the internal

climate variability is in practical terms unpredictable: since its evolution depends on all details of the state of the atmosphere and the ocean (and other subsystems) at a certain point in time, and this detailed knowledge is practically impossible to attain (Schmidt et al., 2011), this is why there are some differences between MPI- ESM-P p2k and MPI-ESM-P. As a result of our study, it seems that effect of the reconstructed volcanic activity rather used in the MPI- ESM-P p2k model rather than the volcanic forcing, seems to be better reflected in our North Aegean alkenone SST, which in turns provides the potential of strengthening the involved models.

6 CONCLUSIONS

This thesis for the paleoceanographic evolution of the North Aegean Sea during the last 4.0 ka was based on alkenone palaeotemperature and proxy reconstructions from M2 high resolution multicore along with data of alkenone Sea Surface Temperature from M3 multicore. Moreover the M2 alkenone SSTs were compared with three different atmospheric model simulations data in annual and seasonal resolution. For the last 4000 years we focused on important periods in the same region that are considered as follows:

- During the Bronze Age (BA) - Iron Age (IA) (2000–586 BC) planktonic foraminifera are dominant suggesting oligotrophic conditions and high productivity surface waters. The period from 1700 to 950 BC is mostly dominated by relative low temperatures that are between 18.5 ºC and 17 ºC. Towards the end of 900 BC alkenone palaeotemperature values change completely indicating a rapid climate change same as in Mayewski et al.(2004) with 5 ºC difference in a duration of 230 years.
- There is lack of data during 600 to 100 BC for this part of the Mediterranean which are going to be analysed in forthcoming research.
- For the time periods between the Roman Warm Period (RWP, before 300 AD) and the Late Antique Little Ice Age (LALIA, 536-around 660 AD) only simulated data by the MPI-ESM-P p2k model are available. Simulated SSTs show warm conditions with a significant decreasing trend of temperature occuring during the first 300 years, and then a marked increase following until the end of the RWP.
- During the Dark Ages (DA, ~300-600 AD) time period, a significant peak in simulated SST anomalies is detected in the middle of 5th century and a rather abrupt decrease, between 550 AD and 600 AD (LALIA) is observed and maybe link to the strong volcanic forcing during that time. During the LALIA the MPI-ESM-P p2k shows warm conditions whereas the alkenone SSTs cold in this occasion either the model might be off, or variability that may be due to natural internal processes within the climate system (internal variability) is more important than in variations of natural or anthropogenic external forcing).”
- During the Medieval Climate Anomaly (MCA) (600 to 1200 AD) period from 500 to 850 AD there is a cooling trend. A progressive decrease of $\delta^{18}O$ values

between 700 AD and 1000 AD matches this evidence and is followed by a rapid increase around 1150 AD. During the MCA all paleo model simulations show anomalous warm climatic conditions. Until 1100 AD relative greater organic production is observed, except for the time interval between 800 AD and 850 AD, where a rather abrupt decrease occurs which correlates with the rapid increase of the SST. From 850 to 950 AD there is higher preservation of organic matter. During the same period there is high supply from continental/riverine runoffs (Gogou et al., 2007; Triantaphyllou et al., 2014; Triantaphyllou et al., 2009). All three model simulations present generally large warm biases.

- During the Little Ice Age (LIA) (1200 to 1850 AD) the $\delta^{18}O$ records cold climate conditions, with two abrupt warm conditions at 1260 AD and 1470 AD, supporting high surface water temperatures and the development of Deep Chlorophyll Maximum (DCM). During the middle of 13^{th}, 15^{th}, 16^{th} century the dominant conditions as reflected by the isotopical analysis are warm and match with the alkenone SST measurements. Primary productivity of the surface water, was enriched in nutrient levels during this coldest LIA period, due to increased vertical mixing and upwelling, which fits well with increased productivity probably associated with vertical mixing. All three model simulations show two cold signals during 1570-1720 AD along with constantly dysoxic conditions.
- The Industrial Period (after 1850 AD) is characterized by an increase of warm water species and has a continuous SST warming trend, interrupted by two cooling events at 1832 AD and 1995 AD. All three models are in agreement with the increasing trend of the reconstructed alkenone SSTs.
- Alkenone-based SST records show a similar pattern as the simulated annual mean SSTs, but independently of the choice of the climate model, we also observe significant mismatches. These differences are linked to the fact that the proxy data records used in this study are located in an area which is challenging to simulate with global climate models due to its complex topography and due to the fact that models give results on a specific area about the dominant atmospheric situation above 2m from the sea whereas the proxy reconstructions are for a specific selected site. The differences between the model simulations are also due to

different forcings, physical implementations, time trajectories and internal variability. The SST is considered to be the mean annual value, through these results and it mostly represents the bloom of *E.huxleyi* during February/March (Triantaphyllou et al., 2010; Triantaphyllou et al., 2004), mostly affected by the winter period. Annual MPI- ESM-P p2k and the alkenone SST values have the highest correlation among the model simulations with 95% statistical significance of low pass filter and is also correlating better for the winter period, summer and autumn. The MPI- ESM-P r1 also correlates better during winter and then during summer when it has the same value with the annual. Effect of the reconstructed volcanic activity rather used in the MPI- ESM-P p2k model rather than the volcanic forcing reflects better in our North Aegean alkenone SST, which in turns provides the potential of strengthening the involved models.

7 MEDCLIVAR 2016 CONFERENCE

Coupling paleoceanographic and paleoclimatic data of the North Aegean for the last 2000 years.

Fatourou M.[1], Xoplaki E.[2] ,Triantaphyllou M.[1], Gogou A.[3], Dimiza M.[1] Parinos C[3]., Luterbacher J.[2]

[1] Faculty of Geology and Geoenvironment, University of Athens, Panepistimioupolis, 157 84 Athens, Greece

[2] Climatology, Climate Dynamics and Climate Change, Department of Geography, Justus-Liebig-University Giessen, Giessen, Germany

[3] Hellenic Centre for Marine Research, Institute of Oceanography, 190 13 Anavyssos, Attiki, Greece

During the last decades, a variety of scientific studies have shown and supported that marine sediments preserve a wealth of information for the reconstruction of ocean and climate history in the form of their microfossil assemblage, organic matter, elemental and isotopic composition of fossils. Nowadays, it is possible to combine data from marine sediment analysis and climatic models to provide even more information about the paleoceanographic and paleoclimatic conditions of an area of interest.

This research focuses on reconstructing past climatic changes of the North Aegean, due to its unique physical and geographic characteristics with the use of climate models and marine fossil analysis.

The high resolution marine record established for the past 1500 years in the North Aegean Sea, Greece (multicore M2, Athos basin, 1018 m depth) was used to provide palaeoclimatic data from the fluctuations of the isotopic signal of the planktonic foraminifer *Globigerinoides ruber*. In addition, changes in dissolved oxygen concentrations in the pore and bottom waters at the same site, were obtained by relative abundance of the benthic foraminiferal low oxygen indicators and the subsequent calculation of Low Oxygen -index.

The climatic model data were provided from the simulations of the Coupled Model Intercomparison Project (CMIP5) for the last 2000 years. In particular, the MPI-ESM-P-p2k, the MPI-ESM-P r1 and the CCSM4 r1 simulations for this specific area were analyzed on annual and seasonal resolution. Via the analysis, short-term changes in temperature and humidity were examined and correlated with the $\delta\ ^{18}O_{G.ruber}$ isotopic signal in relation to alkenone Sea Surface Temperature record, the upper water column Stratification index and the bottom waters Low-Oxygen index. Through this multi proxy methodology the climatic conditions of the Roman Period, the Dark Ages, the Late Antique Little Ice Age, the Medieval Climate Anomaly and the Little Ice Age were sufficiently coupled with the paleoceanographic-paleoclimatic reconstruction for the North Aegean Sea.

MEDCLIVAR 2016 CONF
Athens, Greece Learning from the past, perceiving
26-30 September 2016 the present, engaging for the future

2000 years North Aegean paleoceanographic and paleoclimatic information

Maria Fatourou[1*], Elena Xoplaki[2], Maria Triantaphyllou[1], Alexandra Gogou[3], Margarita Dimiza[1], Constantine Parinos[3], Juerg Luterbacher[2]

(1) University of Athens, Faculty of Geology & Geoenvironment, Panepistimioupolis 15784, Athens, Greece *mfatourou@geol.uoa.gr

(2) Climatology, Climate Dynamics and Climate Change, Department of Geography, Justus-Liebig University Giessen

(3) Hellenic Centre for Marine Research, Institute of Oceanography, Anavyssos, Greece

STUDY AREA, MATERIALS AND METHODS

This research focuses on **reconstructing** and **analyzing** past marine climatic changes of the North Aegean, using **marine fossil** and output of forced **paleo models**. This intercorrelation has enabled an even higher evaluation of recorded climatic changes within the eastern Mediterranean.

Multicore M2 (Athos basin) - North Aegean - 1018 m depth (Fig.1) provides palaeoclimatic information from the isotopic signal fluctuations of the planktonic foraminifer *Globigerinoides ruber* (*alba*) (Fig.2). Changes in dissolved oxygen concentrations in the pore and bottom waters were obtained by relative abundance of the benthic foraminiferal low oxygen indicators and the subsequent calculation of Low Oxygen index (Kuhnt et al., 2007).

Palaeoclimatic model data → simulations of the **Coupled Model Intercomparison Project 5 (CMIP5)** (Fig.3) (Taylor et al., 2012) covering the last **2000** years. The **MPI-ESM-P-p2k**, the **MPI-ESM-P r1** and the **CCSM4 r1** simulations were analyzed on annual and seasonal resolution for temperature.

Short-term changes in temperature were examined and correlated to the alkenone **Sea Surface Temperature record** (SST), the **δ $^{18}O_{G.ruber}$** and **δ ^{13}C** isotopic signal, the upper water column **Stratification index** (S) and the bottom waters **Low-Oxygen index** (LO)

The reconstructed SST data were estimated with a smoothing local adaptive kernel regression (Gogou et al., 2016).
On both the SST and the paleomodel data a 100 years running mean filter was applied.

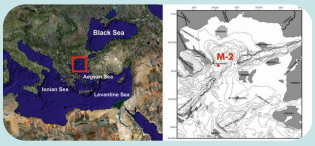

Fig.1: Study area

Anomalies are calculated with respect to the reference period 1500-1850 AD.


Fig.2: *Globigerinoides ruber (alba)*

Fig.3: Northern Aegean model simulations areas

Benthic : **95** sediment samples of 0.5 cm sampling resolution ➔ Hydrogen peroxide and sieved through a 125 μm mesh.
Planktonic (isotope analysis) : **40** samples containing **6** specimens of *Globigerinoides ruber* per sample.

RESULTS

- The abundance LO index (Fig.4) shows relatively **low** values between 4.25 and 26.9 for the sediments → Oxygenated waters
- High values of S-index (Fig.4) indicate relatively deep nutricline/thermocline position, low values imply high paleoproductivity (Flores et al., 2000). M2 core: values vary between 0.11 and 0.69.
- δ^{13}C measurements show how much of the seasonal fluctuations are controlled by the terrestrial biosphere versus oceanic exchange. → positive peaks during 13th, 15th ,16th and 18th century

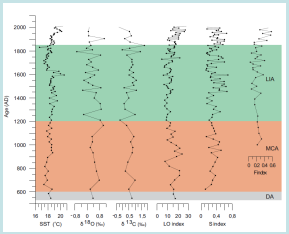

Fig.4: SST(°C), δ $^{18}O_{G.ruber}$(‰), δ ^{13}C(‰), LO index , S index, Forestation(F) cover index.(LIA=Little Ice Age, MCA=Medieval Climate Anomaly, DA=Dark Ages).

Table 1: δ $^{18}O_{G.ruber}$(‰) results

Climatic condition	Century
cold	Until 13th
warm	13th
cold	14th - middle 15th
warm	15th
cold	Ending of 15th
warm	Middle of 16th
cold	Ending of 16th
warm	Beginning and Ending of 17th
Min (-0.66‰) warm	End of 18th
Max (1.07‰) cold	20th

- The northern Aegean SSTs (Figs. 4,5) show a **cold** period during the 7th - early 10th century.
- 10th until middle 11th → **warmer** conditions.

Middle of 11th - end of the 12th century again **cooler** conditions.
Until the middle 17th century → generally above normal SSTs.
From the 2nd half of the 17th century there is a strong **cooling** of approx. 1◦C within a few years.

- Until the mid 19th century SSTs are below the 1500-1800 AD climatology, followed by a strong **warmer** trend.

- Seasonal analysis: SST has more positive correlation during **winter** for the MPI-ESM-P p2k and MPI-ESP-P r1

bloom of *E.huxleyi* during February/March (Triantaphyllou et al., 2010; 2004)

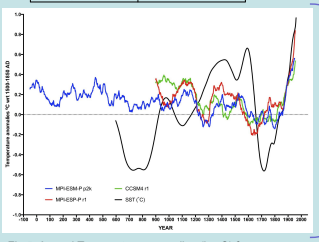

Fig.5: Annual Temperature anomalies (in °C) for different model simulations and comparison with SST.

- MPI-ESP-P r1 and MPI-ESM-P p2k simulations = **warm**
- CCSM4 r1 much more **warmer** values → **10th century**
- Indication of a very **warm** period from all simulations → **13th century**
- Evidence of **cold** climatic signal → **middle 16th – early 18th century**
- MPI-ESP-P r1 shows a **warmer** signal → **18th -19th century**

After 1860 AD the simulations present a **continuous warm** period

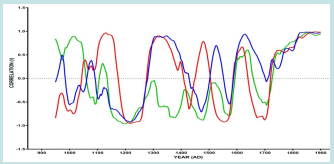
Fig.6: Running correlation between model simulations and SST for winter period(December January February).

Changes in correlation value over time.

References
Flores et al., 2000. Palaeogeogr. Palaeoclimatol. Palaeoecol. 161, 459-478.
Gogou et al., 2016. Quaternary Science Reviews, v. 136, p. 209-228.
Kuhnt et al., 2007. Marine Micropaleontology, v. 64, p. 141-162.
Taylor et al., 2012, Bulletin of the American Meteorological Society, v. 93, p. 485-498.
Triantaphyllou et al., 2004. Micropaleontology 50. 127-144. Triantaphyllou et al. 2010. Geobios 43 99-110.

Acknowledgements
Workshop at the Navarino Environmental Observatory (NEO), Greece (April 2014),Mediterranean Holocene climate and human societies. The workshop was co-sponsored by PAGES, NEO, the MISTRALS/PaleoMex program, the Labex OT-Med, the Bolin Centre for Climate Research at Stockholm University, and the Institute of Oceanography at the Hellenic Centre for Marine Research. Funding was provided by the Greek National Project KRIPIS, the University of Athens Research Project KA 70/4/11078, and the European Research Projects'Medifcon' (MarinERA, EU/FP6) and 'Sea for Society' .R/V Aegaeo (HCMR, Greece)"MEDECOS II" cruise.

8 REFERENCES

Alavi, S.N., 1988, Late Holocene Deep-Sea Benthic Foraminifera from the Sea of Marmara. Mar. Micropaleontol. 13, 213–237.
Altenbach, A.V., and Struck, U., 2001, On the coherence of organic carbon flux and benthic foraminiferal biomass. Journal of Foraminiferal Research, vol. 31, no. 2, pp. 79–85.
Alverson, K., Oldfield, F., and Bradley, R.S.E., 1999, Past Global Changes and Their Significance for the Future. Elsevier, Amsterdam, 479 pp.
Androulidakis, Y.S., Kourafalou, V.H., Krestenitis, Y.N., and Zervakis, V., 2012, Variability of deep water mass characteristics in the North Aegean Sea: the role of lateral inputs and atmospheric conditions. Deep-Sea Res. Part I Oceanogr. Res. Pap. 67, 55-72.
Baumann, K.-H., Cepek, M., and Kinkel, H., 1999, Coccolithophores as indicators of ocean water masses, surface-water temperature, and paleoproductivity: Examples from the South Atlantic. In: Fischer G., Wefer G., Eds, Use of proxies in paleoceanography: Examples from the South Atlantic, 117–144 pp., Springer, Berlin.
Bergamasco, A., and Malanotte-Rizzoli, P., 2010, The circulation of the Mediterranean Sea: a historical review of experimental investigations: Advances in Oceanography and Limnology, v. 1, p. 11-28.
Bernard, J.M., and Sen Gupta, B.K., 1999, Foraminifera of oxygen-depleted environments. In: Sen Gupta, B.K. (Ed.), Modern Foraminifera. Kluwer Academic Publishers, Dordecht, pp. 201–216.
Bernasconi, S.M., and Pika-Biolzi, M., 2000, A stable isotope study of multiple species of planktonic foraminifera across sapropels of the Tyrrhenian Sea, ODP Site 974. Palaeogeography Palaeoclimatology Palaeoecology 158,281–292.
Boltovskoy, D., 1998, Classification and distribution of South Atlantic Recent Polycystine Radiolaria. Paleontologica Electronica 1, 1–116.
Bond, G., Kromer, B., Beer, J., Muscheler, R., Evans, M.N., Showers, W., Hoffmann, S., Lotti-Bond, R., Hajdas, I., and Bonani, G., 2001, Persistent solar influence on North Atlantic climate during the Holocene, Science, 294, 2130–2136, doi:10.1126/science.1065680.
Bothe, O., Jungclaus, J.H., and Zanchettin, D., 2013, Consistency of the multi-model CMIP5/PMIP3-past1000 ensemble: Climate of the Past, v. 9, p. 2471-2487.
Boyd, P.W., and Doney, S.C., 2002, Modelling regional responses by marine pelagic ecosystems to global climate change. Geophysical Research Letters 29, 53–56.
Bradley, R.S., 1999, Paleoclimatology. Reconstructing the climates of the Quaternary (2nd edn.), International Geophysics (vol. 64). San Diego: Academic Press.
—, 2015, Paleoclimatology : reconstructing climates of the Quaternary.Third edition. ISBN 978-0-12-386913-5.
Bradley, R.S., and Eddy, J.A., 1991, Records of past global changes. In: Bradley, R.S. (Ed.), Global Changes of the Past.: University Corporation for Atmospheric Research, Boulder, pp. 5–9.
Büntgen, U., Myglan, V.S., Ljungqvist, F.C., McCormick, M., Di Cosmo, N., Sigl, M., Jungclaus, J., Wagner, S., Krusic, P.J., Esper, J., Kaplan, J.O., de Vaan, M.A.C.,

Luterbacher, J., Wacker, L., Tegel, W., and Kirdyanov, A.V., 2016, Cooling and societal change during the Late Antique Little Ice Age from 536 to around 660 AD: Nature Geoscience, v. 9, p. 231-236.

Cacho, I., Grimalt, J.O., Canals, M., Sbaffi, L., Shackleton, N.J., Schönfeld, J., and Zahn, R., 2001, Variability of the western Mediterranean Sea surface temperature during the last 25,000 years and its connection with the Northern Hemisphere climatic changes. Paleoceanography 16,40–52.

Camuffo, D., Bertolin, C., Barriendos, M., Dominguez-Castro, F., Cocheo, C., Enzi, S., Sghedoni, M., Valle, A., Garnier, E., Alcoforado, M.J., Xoplaki, E., Luterbacher, J., Diodato, N., Maugeri, M., Nunes, M.F., and Rodriguez, R., 2010, 500-years temperatura reconstruction in the Mediterranean Basin by means of documentary data and instrumental observations, Climatic Change, 101, 169–199.

Conte, M.H., Sicre, M.A., Rühlemann, C., Weber, J.C., Schulte, S., Schulz-Bull, D., and Blanz, T., 2006, Global temperature calibration of the alkenone unsaturation index (U 37 k) in surface waters and comparison with surface sediments. Geochem. Geophys. Geosystems 7.

Coplen, T.B., 1994, Reporting of stable hydrogen, carbon, and oxygen isotopic abundances ‐ – Technical Report.International Union of Pure and Applied Chemistry, v. 66, p. 273-276.

Corliss, B.H., 1980, Vertical distribution of foraminifera off the coast of Northumberland, England. Journal of Foraminiferal Research, vol. 10, pp. 75–78.

Corte-Real, J., Xuebin, Z., and Xiaolan, W., 1995, Large-scale circulation regimes and surface climatic anomalies over the Mediterranean. Int. J. Climatol. 15, 1135e1150.

Cowie, J., 2013, Climate change: biological and human aspects. Cambridge University Press, p. 582. ISBN 978-1-107-60356-1.

Crowley, T.J., and Unterman, M.B., , , 2013, Technical details concerning development of a 1200 yr proxy index for global volcanism.: Earth Syst. Sci. Data 5, p. 187-197.

de Vernal, A., Eynaud, F., Henry, M., Hillaire-Marcel, C., Londeix, L., Mangin, S., Matthiessen, J., Marret, F., Radi, T., Rochon, A., Solignac, S., and Turon, J., 2005, Reconstruction of sea-surface conditions at middle to high-latitudes of the Northern Hemisphere during the Last Glacial Maximum (LGM) based on dinoflagellate cyst assemblages. Quat. Sci. Rev. 24, 897–924.

de Vernal, A., Hillaire-Marcel, C., Thuron, J.-L., and Matthiessen, J., 2000, Reconstruction of sea-surface temperature, salinity and sea-ice cover in the northern Atlantic during the last glacial maximum based on dinocyst assemblages. Can. J. Earth Sci. 37, 725–750.

Dimiza, M., Koukousioura, O., Triantaphyllou, M., and Dermitzakis, M., 2016, Live and dead benthic foraminiferal assemblages from coastal environments of the Aegean Sea (Greece): Distribution and diversity.Revue de micropaléontologie 59 (2016) 19–32.

Dimiza, M., Triantaphyllou, M., Malinverno, E., Psarra, S., Karatsolis, B.-T., Mara, P., Lagaria, A., and Gogou, A., 2015, The composition and distribution of living coccolithophores in the Aegean Sea (NE Mediterranean). Micropaleontology [Internet]. 2015;61(6):521-540.

Emeis, K.-C., Struck, U., Schulz, H.-M., Rosenberg, R., Bernasconi, S., Erlenkeuser, H., Sakamoto, T., and Martinez-Ruiz, F., 2000, Temperature and salinity variations of Mediterranean Sea surface waters over the last 16,000 years from records of planktonic stable oxygen isotopes and alkenone unsaturation ratios: Palaeogeography, Palaeoclimatology, Palaeoecology, v. 158, p. 259-280.

Emeis, K.C., Schulz, H.M., Struck, U., Sakamoto, T., Doose, H., Erlenkeuser, H., Howell, M., Kroon, D., and Paterne, M., 1998, Stable isotope and alkenone temperature records of sapropels from sites 964 and 967: Constraining the physical environment of sapropel formation in the Eastern Mediterranean Sea. Proc. Ocean Drill. Program Sci. Res. 60, 309–331.

Esper, J., Frank, D., Büntgen, U., Verstege, A., Luterbacher, J., and Xoplaki, E., 2007, Long-term drought severity variations in Morocco. Geophys. Res. Lett. 34.

Fischer, G., and Wefer, G., 1999, Use of proxies in paleoceanography. Examples from the South Atlantic. Berlin: Springer.

Flores, J.A., Barcena, M.A., and Sierro, F.J., 2000, Ocean-surface and wind dynamics in the Atlantic Ocean off Northwest Africa during the last 140 000 years. Palaeogeogr. Palaeoclimatol. Palaeoecol. 161, 459-478.

Gao, C., Robock, A., and Ammann, C.J., 2008, Volcanic forcing of climate over the last 1500 years: an improved ice coreebased index for climate models. : Geophys. Res.113, D23111.

Giorgetta, M.A., Jungclaus, J.H., Reick, C.H., Legutke, S., Bader, J., Böttinger, M., Brovkin, V., Crueger, T., Esch, M., Fieg, K., Glushak, K., Gayler, V., Haak, H., Hollweg, H.-D., Ilyina, T., Kinne, S., Kornblueh, L., Matei, D., Mauritsen, T., Mikolajewicz, U., Mueller, W., Notz, D., Pithan, F., Raddatz, T., Rast, S., Redler, R., Roeckner, E., Schmidt, H., Schnur, R., Segschneider, J., Six, K.D., Stockhause, M., Timmreck, C., Wegner, J., Widmann, H., Wieners, K.-H., Claussen, M., Marotzke, J., and Stevens, B., 2013, Climate and carbon cycle changes from 1850 to 2100 in MPI-ESM simulations for the coupled model intercomparison project phase 5: Journal of Advances in Modeling Earth Systems, v. 5, p. 572-597.

Giorgi, F., 2002a, Variability and trends of sub-continental scale surface climate in the twentieth century. Part I: observations. Clim. Dyn., 18, 675–691. .

Giorgi, F., and Lionello, P., 2008, Climate change projections for the Mediterranean region: Global and Planetary Change, v. 63, p. 90-104.

Gogou, A., Bouloubassi, I., Lykousis, V., Arnaboldi, M., Gaitani, P., and Meyers, P.A., 2007, Organic geochemical evidence of Late Glacial–Holocene climate instability in the North Aegean Sea: Palaeogeography, Palaeoclimatology, Palaeoecology, v. 256, p. 1-20.

Gogou, A., Bouloubassi, I., and Stephanou, E., 2000, Marine organic geochemistry of the Eastern Mediterranean: 1. Aliphatic and polyaromatic hydrocarbons in Cretan Sea surficial sediments. : Mar Chem 68:265–282.

Gogou, A., Triantaphyllou, M., Xoplaki, E., Izdebski, A., Parinos, C., Dimiza, M., Bouloubassi, I., Luterbacher, J., Kouli, K., Martrat, B., Toreti, A., Fleitmann, D., Rousakis, G., Kaberi, H., Athanasiou, M., and Lykousis, V., 2016, Climate variability and socio-environmental changes in the northern Aegean (NE

Mediterranean) during the last 1500 years: Quaternary Science Reviews, v. 136, p. 209-228.
Gooday, A.J., 1994, The biology of deep-sea Foraminifera: a review of some advances and their applications in paleoceanography. Palaios 9, 14–31.
—, 2003, Benthic Foraminifera (Protista) as tools in deep- water paleoceanography: environmental influences of faunal char- acteristics. Advances in Marine Biology, vol. 46, pp. 1–90.
Goudeau, M.L.S., Reichart, G.J., Wit, J.C., deNooijer, L.J., Grauel, A.L., Bernasconi, S.M., and de Lange, G.J., 2015, Seasonality variations in the Central Mediterranean during climate change events in the Late Holocene. Palaeogeogr. Palaeoclimatol. Palaeoecol. 418, 304–318. .
Grauel, A.-L., Goudeau, M.-L.S., de Lange, G.J., and Bernasconi, S.M., 2013a, Climate of the past 2500 years in the Gulf of Taranto, central Mediterranean Sea: A high-resolution climate reconstruction based on δ18O and δ13C of Globigerinoides ruber (white).The Holocene vol. 23 no. 10 1440-1446
Grauel, A.-L., Leider, A., Goudeau, M.-L.S., Müller, I., Bernasconi, S.M., Hinrichs, K.-U., de Lange, G.J., Zonneveld, K.A.F., and J.M., V.G., 2013b, What do SST proxies really tell us? A high-resolution multiproxy (UK'37, TEXH86 and foraminifera d18O) study in the Gulf of Taranto, central Mediterranean Sea. Quaternary Science Reviews, 73, 115-131.
Hemleben, C., Spindler, M., and Anderson, O.R., 1989, Modern Planktonic Foraminifera. Springer-Verlag, New York, p. 363.
Henderson, G.M., 2002, New proxies for paleoclimate. Earth Planet. Sci. Lett., 203, 1–13.
Herbert, T.D., 2003, Alkenone paleotemperature determinations. In: Holland, D.H., Turekian, K.K. (Eds.), Treatise on Geochemistry. Pergamon, Oxford, pp. 391-432.
Hoerling, M., Eischeid, J., Perlwitz, J., Quan, X., Zhang, T., and Pegion, P., 2012, On the increased frequency of Mediterranean drought, J. Climate, 25, 2146–2161.
Holzwarth, U., Esper, O., and Zonneveld, K.A.F., 2010, Organic-walled dinoflagellate cysts as indicators of oceanographic conditions and terrigenous input in the NW African upwelling region. Review of Palaeobotany and Palynology 159(1–2), 35–55.
Horvath, F., and Berckhemer, H., 1982, Mediterranean backarc basins. In: Berckhemer, H., Hsü, K.J. (Eds.), Alpine Mediterranean Geodynamics: Am. Geophys. Un., Geodynamics Series, vol. 7, pp. 141–173.
Ignatiades, L., Psarra, S., Zervakis, V., Pagou, K., Souvermezoglou, E., Assimakopoulou, G., and Gotsis-Skretas, O., 2002, Phytoplankton size- based dynamics in the Aegean Sea (Eastern Mediterranean). J Mar Syst 36:11–28.
Incarbona, A., Bonomo, S., Di Stefano, E., Zgozi, S., Essarbout, N., Talha, M., Tranchida, G., Bonanno, A., Patti, B., Placenti, F., Buscaino, G., Cuttitta, A., Basilone, G., Bahri, T., Massa, F., Censi, P., and Mazzola, S., 2008, Calcareous nannofossil surface sediment assemblages from the Sicily Channel (central Mediterranean Sea): palaeoceanographic implications. Mar. Micropaleontol. 67,297-309.

Incarbona, A., Ziveri, P., Di Stefano, E., Lirer, F., Mortyn, G., Patti, B., Pelosi, N., Sprovieri, M., Tranchida, G., Vallefuoco, M., Albertazzi, S., Bellucci, L.G., Bonanno, A., Bonomo, S., Censi, P., Ferraro, L., Giuliani, S., Mazzola, S., and Sprovieri, R., 2010, The impact of the Little Ice Age on Coccolithophores in the central Mediterranean Sea. Clim. Past 6, 795–805.

IPCC, 2007, Intergovernmental Panel on Climate Change fourth assessment report on scientific aspects of climate change for researchers, students, and policymakers.

—, 2013, Annex III: glossary, Planton, S. (Ed.). In: Stocker, T. et al. (Eds.), Climate Change 2013: the Physical Science Basis. Contribution of Working Group I to the Fifth Assessment Report of the Intergovernmental Panel on Climate Change.Cambridge University Press, Cambridge, United Kingdom and New York, NY, USA.

Jorissen, F.J., 1999, Benthic foraminiferal microhabitats below the sediment-water interface. In: Sen Gupta,B.K.,ed., Modern Foraminifera. Dordrecht: Kluwer, pp. 161–179.

Jorissen, F.J., Fontanier, C., and Thomas, E., 2007, Paleoceanographical proxies based on deep-sea benthic foraminiferal assemblage characteristics. In: Hillaire-Marcel C., de Vernal A., Eds, Proxies in Late Cenozoic Paleoceanography, 263–226 pp., Developments in Marine Geology, 1, Elsevier, Amsterdam, The Netherlands.

Jungclaus, J.H., Lohmann, K., and Zanchettin, D., 2014, Enhanced 20th-century heat transfer to the Arctic simulated in the context of climate variations over the last millennium. Clim. Past 10, 2201-2213. .

Kleijne, A., 1993, Morphology, Taxonomy and Distribution of Extant Coccolithophorids (Calcareous Nannoplankton), Vrije Universiteit, 320 pp.

Knappertsbusch, M.W., 1990, Geographic distribution of modern coccolithophores in the Mediterranean Sea and morphological evolution of Calcidiscus leptoporus. Unpub. Ph.D. dissertation, Swiss Federal Inst. Of Tech., Zurich ETH, Nr. 9169.

Kouli, K., Gogou, A., Bouloubassi, I., Triantaphyllou, M.V., Ioakim, C., Katsouras, G., Roussakis, G., and Lykousis, V., 2012, Late postglacial paleoenvironmental change in the northeastern Mediterranean region: Combined palynological and molecular biomarker evidence: Quaternary International, v. 261, p. 118-127.

Kuhnt, T., Schmiedl, G., Ehrmann, W., Hamann, Y., and Andersen, N., 2008, Stable isotopic composition of Holocene benthic foraminifers from the Eastern Mediterranean Sea: Past changes in productivity and deep water oxygenation. Palaeogeography Palaeoclimatology Palaeoecology 268, 106–115.

Kuhnt, T., Schmiedl, G., Ehrmann, W., Hamann, Y., and Hemleben, C., 2007, Deep-sea ecosystem variability of the Aegean Sea during the past 22 kyr as revealed by Benthic Foraminifera: Marine Micropaleontology, v. 64, p. 141-162.

Landrum, L., Otto-Bliesner, B.L., Wahl, E.R., Conley, A., Lawrence, P.J., Rosenbloom, N., and Teng, H., 2013, Last Millennium Climate and Its Variability in CCSM4: Journal of Climate, v. 26, p. 1085-1111.

Lavigne, F., Degeai, J.-P., Komorowski, J.-C., Guillet, S., Robert, V., Lahitte, P., Oppenheimer, C., Stoffel, M., Vidal, C.M., Surono, P., I., , Wassmer, P., Hajdas, I., Sri Hadmoko, D., and de Beliza, E., 2013, Source of the great A.D. 1257 mystery eruption unveiled, Samalas volcano, Rinjani Volcanic Complex, Indonesia. Proc. Natl. Acad. Sci. U. S. A. 110, 6742-16747.

Le Pichon, X., and Angelier, J., 1979, The Hellenic arc and trench system: a key to the neotectonic evolution of the eastern Mediterranean area. Tectonophysics 60, 1–42.

Ledru, M.-P., Jomelli, V., Samaniego, P., Vuille, M., Hidalgo, S., Herrera, M., and Ceron, C., 2013, The Medieval Climate Anomaly and the Little Ice Age in the eastern Ecuadorian Andes. Clim. Past 9, 307-321. http://dx.doi.org/10.5194/cp-9-307- 2013.

Lionello, P., Malanotte-Rizzoli, P., Boscolo, R., Alpert, P., Artale, V., Li, L., Luterbacher, J., May, W., Trigo, R., Tsimplis, M., Ulbrich, U., and Xoplaki, E., 2006, The Mediterranean climate: an overview of the main characteristics and issues. Dev. Earth Environ. Sci. 1-26.

Lirer, F., Sprovieri, M., Vallefuoco, M., Ferraro, L., Pelosi, N., Giordano, L., and Capotondi, L., 2014, Planktonic foraminifera as bio-indicators for monitoring the climatic changes that have occured over the past 2000 years in the southeastern Tyrrhenian Sea.Integrative Zoology Volume 9, Issue 4, pages 542–554.

Loeblich, A.R., and Tappan, H., 1987, Foraminiferal Genera and their Classification. Van Nostrand Rienhold Co., New York.

—, 1994, Foraminifera of the Sahul Shelf and Timor Sea. Cushman Foundation for Foraminiferal Research, Special Publication, 31: 1-661.

Lohmann, G., Pfeiffer, M., Laepple, T., Leduc, G., and Kim, J.-H., 2013, A model–data comparison of the Holocene global sea surface temperature evolution.Clim. Past, 9, 1807–1839.doi:10.5194/cp-9-1807-2013.

Luterbacher, J., García-Herrera, R., Akcer-On, S., Allan, R., Alvarez-Castro, M.-C., Benito, G., Booth, J., Büntgen, U., Cagatay, N., Colombaroli, D., Davis, B., Esper, J., Felis, T., Fleitmann, D., Frank, D., Gallego, D., Garcia-Bustamante, E., Glaser, R., Gonzalez-Rouco, F.J., Goosse, H., Kiefer, T., Macklin, M.G., Manning, S.W., Montagna, P., Newman, L., Power, M.J., Rath, V., Ribera, P., Riemann, D., Roberts, N., Sicre, M.-A., Silenzi, S., Tinner, W., Tzedakis, P.C., Valero-Garcés, B., van der Schrier, G., Vannière, B., Vogt, S., Wanner, H., Werner, J.P., Willett, G., Williams, M.H., Xoplaki, E., Zerefos, C.S., and Zorita, E., 2012, A Review of 2000 Years of Paleoclimatic Evidence in the Mediterranean, The Climate of the Mediterranean Region, Elsevier, p. 87-185.

Luterbacher, J., and Xoplaki, E., 2003, 500-Year Winter temperature and precipitation variability over the mediterranean area and its connection to the large-scale atmospheric circulation. In: Bolle, H.-J. (Ed.), Mediterranean Climate. Variability and Trends. Springer Verlag, Berlin, Heidelberg, pp. 133-153.

Lyberis, N., 1984, Tectonic evolution of the North Aegean trough. In: The Geological Evolution of the Eastern Mediterranean. Dixon J.E. & Robertson A.H.F. (eds.). Oxford: Blackwell Scientific Publ. Geol. Soc. Sp. Publ., 17: 709-725.

Lykousis, V., Chronis, G., Tselepides, A., Price, N., Theocharis, A., Siokou-Fragou, I., Wambeke, F., Danovaro, R., Stavrakakis, S., Duineveld, G., Georgopoulos, D., Ignatiades, L., Souvermezoglou, A., and Voutsinou- Taliadouri, F., 2002, Major outputs of the recent multidisciplinary biogeochemical researches undertaken in the Aegean Sea. : J Mar Syst 33(34):313–334.

Malanotte-Rizzoli, P., Manca, B., Ribera D'Alcalà, M., Theocharis, A., Bergamasco, A., Bregant, D., Budillon, G., Civitarese, G., Georgopoulos, D., Michelato, A.,

Sansone, E., Scarazzato, P., and Souvermezoglou, E., 1997, A synthesis of the Ionian Sea hydrography, circulation and water mass pathways during POEM Phase I, Progr. Oceanogr., 39, 153–204.

Malinverno, E., Karatsolis, B., Dimiza, M.D., Psarra, S., Lagaria, A., and Triantaphyllou, M.V., 2016, Extant silicoflagellates from the North Aegean (eastern Mediterranean Sea): morphologies and double skeletons. Revue de Micropaléontologie, 59/3: 253–265.

Margaritelli, G., Vallefuoco, M., Di Rita, F., Capotondi, L., Bellucci L.G., Insinga, D.D., Petrosino, P., Bomono, S., Cacho, I., Cascella, A., Ferraro, L., Florindo, F., Lubritto, C., Lurcock, P.C., Magri, D., Pelosi, N., Rettori, R., and Lirer, F., 2016, Marine response to climate changes during the last five millennia in the central Mediterranean Sea. Global and Planetary Change, 142, 53–72.

Marlowe, I.T., Brassell, S.C., Eglinton, G., and Green, J.C., 1990, Long-Chain Alkenones and Alkyl Alkenoates and the Fossil Coccolith Record of Marine Sediments, Chem. Geol., 88, 349–375.

Marlowe, I.T., Green, J.C., Neal, A.C., Brassell, S.C., Eglinton, G., and Course, P.A., 1984, Long chain (n-C37-C39) alkenones in the Prymnesiophyceae, distribution of alkenones and other lipids and their taxonomic significance. Brit. Phycolog. J. 19, 203-216.

Martrat, B., Grimalt, J.O., Lopez-Martinez, C., Cacho, I., Sierro, F.J., Flores, J.A., Zahn, R., Canals, M., Curtis, J.H., and Hodell, D.A., 2004, Abrupt temperature changes in the western Mediterranean over the past 250,000 years. Science 306, 1762–1765. .

Mayewski, P.A., Rohling, E.E., Curt Stager, J., Karlén, W., Maasch, K.A., David Meeker, L., Meyerson, E.A., Gasse, F., van Kreveld, S., Holmgren, K., Lee-Thorp, J., Rosqvist, G., Rack, F., Staubwasser, M., Schneider, R.R., and Steig, E.J., 2004, Holocene climate variability: Quaternary Research, v. 62, p. 243-255.

McIntyre, A., and Bé, A.W.H., 1967, Modern coccolithophores of the Atlantic Ocean –I. Placolith and cyrtoliths. Deep-Sea Research 14, 561–597.

Moreno, A., Perez, A., Frigola, J., Nieto-Moreno, V., Rodrigo-Gamiz, M., Martrat, B., Gonzalez-Samperiz, P., Morellon, M., Martín-Puertas, C., Corella, J.P., Belmonte, A., Sancho, C., Cacho, I., Herrera, G., Canals, M., Grimalt, J.O., Jimenez- Espejo, F., Martínez-Ruiz, F., Vegas-Vilarrúbia, T., and Valero-Garces, B.L., 2012, The Medieval Climate Anomaly in the Iberian Peninsula reconstructed from marine and lake records. Quat. Sci. Rev. 43, 16-32.

Mothes, P.A., and Hall, M.L., 2008, The Plinian fallout associated with Quilotoa's 800yr BP eruption, Ecuadorian Andes.J.Volanol. Geotherm. Res. 176, 56-69.

Müller, P.J., Kirst, G., Ruhland, G., von Storch, I., and Rosell-Melé, A., 1998, Calibration of the alkenone paleotemperature index UK’37 based on core-tops from the eastern South Atlantic and the global ocean (60oN - 60oS). Geochim. Cosmochim. Acta 62, 1757-1772.

Murray, J.W., 1991, Ecology and Palaeoecology of Benthic Foraminifera. Longman,London, 397 pp.

Negri, A., Capotondi, L., and Keller, J., 1999, Calcareous nannofossils, planktonic foraminifera and oxygen isotopes in the late Quaternary sapropels of the Ionian Sea. Marine Geology 157, 89–103.

Nieto-Moreno, V., 2012, Late Holocene climatic variability in the western Mediterranean: an integrated organic and inorganic multyproxy approach.PhD 187 pp.

Nieto-Moreno, V., Martínez-Ruiz, F., Giralt, S., Jiménez-Espejo, F., Gallego-Torres, D., Rodrigo-Gámiz, M., García-Orellana, J., Ortega-Huertas, M., and de Lange, G.J., 2011, Tracking climate variability in the western Mediterranean during the Late Holocene: a multiproxy approach: Climate of the Past, v. 7, p. 1395-1414.

Nieto-Moreno, V., Martínez-Ruiz, F., Willmott, V., García-Orellana, J., Masque, P., and Sinninghe Damste, J.S., 2013, Climate conditions in the westernmost Mediterranean over the last two millennia: an integrated biomarker approach. Org. Geochem. 55, 1-10.

Nikulin, G., Kjellström, E., Hansson, U., Strandberg, G., and Ullerstig, A., 2011, Evaluation and future projections of temperature, precipitation and wind extremes over Europe in an ensemble of regional climate simulations, Tellus, 63, 41–55, doi:10.1111/j.1600-0870.2010.00466.x.

Oppenheimer, C., 2003, Climatic, environmental and human consequences of the largest known historic eruption: Tambora volcano (Indonesia) 1815. Prog. Phys. Geogr. 27, 230-259.

Pawlowski, J., and Holzmann, M., 2008, Diversity and geographic distribution of benthic foraminifera: a molecular perspective. Biodviersity and Conservation, vol. 17, pp. 317–328.

Piva, A., Asioli, A., Trincardi, F., Schneider, R.R., and Vigliotti, L., 2008a, Late Holocene climate variability in the Adriatic Sea (Central Mediterranean). The Holocene 18, 153–167. .

—, 2008b, Late-Holocene climate variability in the Adriatic Sea (Central Mediterranean). Holocene 18, 153–167.

Poulos, S., Drakopoulos, P., and Collins, M., 1997, Seasonal variability in sea surface oceanographic conditions in the Aegean Sea (Eastern Mediterranean): an overview. : J Mar Syst 13:225–244.

Pujol, C., and Vergnaud Grazzini, C., 1995, Distribution of live planktic fora- minifers as related to regional hydrography and productive systems of the Mediterranean Sea. Mar Micropaleontol 25:187–217.

Reimer, P.J., and McCormac, F.G., 2002, Marine radiocarbon reservoir corrections for the Mediterranean and Aegean Seas. Radiocarbon 44, 159-166.

Reynolds, C.S., 2006, Ecology of phytoplankton. Cambridge University Press, Cambridge, 535 pp.

Ribera, P., Garcia, R., Diaz, H.F., Gimeno, L., and Hernandez, E., 2000, Trends and interannual oscillations in the main sea-level surface pressure patterns over the Mediterranean, 1955-1990. Geophys. Res. Lett. 27, 1143-1146.

Roberts, N., Moreno, A., Valero-Garcés, B.L., Corella, J.P., Jones, M., Allcock, S., Woodbridge, J., Morellón, M., Luterbacher, J., Xoplaki, E., and Türkeş, M., 2012, Palaeolimnological evidence for an east–west climate see-saw in the Mediterranean since AD 900: Global and Planetary Change, v. 84-85, p. 23-34.

Robertson, A.H.F., Clift, P.D., Degnan, P.J., and Jones, G., 1991, Palaeogeographic and palaeotectonic evolution of the eastern Mediterranean Neotethys. In: Channell,

J.E.T., Winterer, E.L., Jansa, L.F. (Eds.), Palaeogeography and Paleoceanography of Tethys: Palaeogeog., Palaeoclim., Palaeoecol., vol. 87, pp. 289–343.
Robinson, A.R., Golnaraghi, M., Leslie, W.G., Artegiani. A., Hecht, A., Lazzoni, E., Michelato, A., Sansone. E., Theocharis, A., and Unluata, U., 1991, The eastern Mediterranean general circulation: features, structures and variability, Dynam. Atmos. Oceans, 15, 215–240.
Roether, W., Klein, B., Manca, B.B., Theocharis, A., and Kioroglou, S., 2007, Transient Eastern Mediterranean deep waters in response to the massive dense-water output of the Aegean Sea in the 1990s. Prog. Oceanogr. (74), 540–571.
Roether, W., Roussenov, V., and Well, R., 1994, A tracer study of the thermohaline circulation of the Eastern Mediterranean, in Ocean Processes in Climate Dynamics: Global and Mediterranean Examples
P. Malanotte-Rizzoli and A.R. Robinson, eds., Kluwer Academic Publishers, The Netherlands, v. 419, p. 371-394.
Rohling, E., and Cooke, S., 1999, Stable oxygen and carbon isotopes in foraminiferal carbonate shells. In: Barum, K., Gupta, S. (Eds.), Modern foraminifera. Kluwer Academic.
Rohling, E.J., 2007, Oxygen isotope composition of seawater: Encyclopedia of Quaternary Science, p. 1748-1756.
Rohling, E.J., Marino, G., and Grant, K.M., 2015, Mediterranean climate and oceanography, and the periodic development of anoxic event(sapropels). Earth Sci. Rev. 143, 62-97.
Roussakis, G., Karageorgis, A.P., Conispoliatis, N., Lykousis, V., 2004, Last glacial-Holocene sediment sequences in N. Aegean basins: Structure, accumulation rates and clay mineral distribution.: Geo-Mar. Lett. 24, , p. 97-111.
Sangiorgi, F., Capotondi, L., and Brinkhuis, H., 2002, A centennial scale organic-walled dinoflagellate cyst record of the last deglaciation in the South Adriatic Sea (Central Mediterranean). Palaeogeography Palaeoclimatology Palaeoecology 186, 199-216.
Schilman, B., Bar-Matthews, M., Almogi-Labin, A., and Luz, B., 2011, Global climate instability reflected by Eastern Mediterranean marine records during the late Holocene. Palaeogeogr. Palaeoclimatol. Palaeoecol. 176, 157–176. .
Schilman, B., Bar-Matthews, M., Almogilabin, A., and Luz, B., 2001, Global climate instability reflected by Eastern Mediterranean marine records during the late Holocene.Palaeogeogr. Palaeoclimatol. Palaeoecol. 176, 157–176.
Schmidt, G.A., Jungclaus, J.H., Ammann, C.M., Bard, E., Braconnot, P., Crowley, T.J., Delaygue, G., Joos, F., Krivova, N.A., Muscheler, R., Otto-Bliesner, B.L., Pongratz, J., Shindell, D.T., Solanki, S.K., Steinhilber, F., and Vieira, L.E.A., 2011, Climate forcing reconstructions for use in PMIP simulations of the last millennium (v1. 0). Geoscientific Model Development, v. 4, p. 33-45.
—, 2012, Climate forcing reconstructions for use in PMIP simulations of the Last Millennium (v1.1): Geoscientific Model Development, v. 5, p. 185-191.
Schurer, A.P., Tett, S.F.B., and Hegerl, G.C., 2013, Small influence of solar variability on climate over the past millennium. Nat. Geosci. http://dx.doi.org/10.1038/NGEO2040.

Sen Gupta, B.K., and Machain-Castillo, M.L., 1993, Benthic foraminifera on oxygen-poor habitats. Mar. Micropaleontol. 20, 183–201.
Sigl, M., Winstrup, M., McConnell, J.R., Welten, K.C., Plunkett, G., Ludlow, F., Büntgen, U., Caffee, M., Chellman, N., Dahl-Jensen, D., Fischer, H., Kipfstuhl, S., Kostick, C., Maselli, O.J., Mekhaldi, F., Mulvaney, R., Muscheler, R., Pasteris, D.R., Pilcher, J.R., Salzer, M., Schüpbach, S., Steffensen, J.P., Vinther, B.M., and Woodruff, T.E., 2015, Timing and climate forcing of volcanic eruptions for the past 2,500 years.: Nature, v. 523, p. 543-9.
Sisma-Ventura, G., Guzner, B., Yam, R., Fine, M., and Shemesh, A., 2009, The reef builder gas- tropod Dendropoma petraeum—a proxy of short and long term climatic events in the Eastern Mediterranean. Geochim. Cosmochim. Acta 73, 4376–4381.
Skliris N., Sofianos S., Gkanasos A., Mantziafou A., Vervatis V., Axaopoulos P., and A., L., 2012, Decadal scale variability of sea surface temperature in the Mediterranean Sea in relation to atmospheric variability, Ocean Dynam., 62 (1), 13–30, http://dx.doi.org/10.1007s10236-011-0493-5.
Smith, R.D., P. Jones, P., Briegleb, B., Bryan, F., Danabasoglu, G., Dennis, J., Dukowicz, J., Eden, C., Fox-Kemper, B., Gent, P., Hecht, M., Jayne, S., Jochum, M., Large, W., Lindsay, K., Maltrud, M., Norton, N., Peacock, S., Vertenstein, M., and Yeager, S., 2010, The Parallel Ocean Program (POP) reference manual. Los Alamos National Laboratory Tech. Rep. LAUR-10-01853, 141 pp.
SoHelME, 2005, E. Papathanassiou & A. Zenetos (eds) State of the Hellenic Marine Environment, p. 360.
Sprovieri, M., Tranchida, G., Vallefuoco, M., Albertazzi, S., Bellucci, L.G., Bonanno, A., Bonomo, S., Censi, P., Ferraro, L., Giuliani, S., Mazzola, S., and Sprovieri, R., 2010, The impact of the Little Ice Age on Coccolithophores in the central Mediterranean Sea. Clim. Past 6, 795–805.
Steinhilber, F., Beer, J., and Fröhlich, C., 2009, Total solar irradiance during the Holocene. Geophys. Res. Lett. 36, L19704.
Stott, P.A., et al.,, 2000, External control of 20th century temperature by natural and anthropogenic forcings. Science 290 (5499), 2133-2137.
Taylor, K.E., Stouffer, R.J., and Meehl, G.A., 2012, An Overview of CMIP5 and the Experiment Design: Bulletin of the American Meteorological Society, v. 93, p. 485-498.
Theocharis, A., Nittis, H., Kontoyiannis, E., Papageorgiou, E., and Balopoulos, E., 1999, Climatic changes in the Aegean Sea influence the Eastern Mediterranean thermohaline circulation (1986–1997). : Geophys Res Lett 26(11):1617–1620.
Toohey, M., Krüger, K., Sigl, M., Stordal, F., and Svensen, H., 2016, Climatic and societal impacts of a volcanic double event at the dawn of the Middle Ages. Climatic Change (2016) 136:401–412 DOI 10.1007/s10584-016-1648-7.
Triantaphyllou, M., Dimiza, M., Krasakopoulou, E., Malinverno, E., Lianou, V., and Souvermezoglou, E., 2010, Seasonal variation in *Emiliania huxleyi* coccolith morphology and calcification in the Aegean Sea (Eastern Mediterranean).Geobios 43 99-110.
Triantaphyllou, M.V., Antonarakou, A., Kouli, K., Dimiza, M., Kontakiotis, G., Papanikolaou, M.D., Ziveri, P., Mortyn, P.G., Lianou, V., Lykousis, V., and

Dermitzakis, M.D., 2009a, Late Glacial–Holocene ecostratigraphy of the south-eastern Aegean Sea, based on plankton and pollen assemblages: Geo-Marine Letters, v. 29, p. 249-267.

Triantaphyllou, M.V., Gogou, A., Bouloubassi, I., Dimiza, M., Kouli, K., Rousakis, G., Kotthoff, U., Emeis, K.-C., Papanikolaou, M., Athanasiou, M., Parinos, C., Ioakim, C., and Lykousis, V., 2014, Evidence for a warm and humid Mid-Holocene episode in the Aegean and northern Levantine Seas (Greece, NE Mediterranean): Regional Environmental Change, v. 14, p. 1697-1712.

Triantaphyllou, M.V., Gogou, A., Dimiza, M.D., Kostopoulou, S., Parinos, C., Roussakis, G., Geraga, M., Bouloubassi, I., Fleitmann, D., Zervakis, V., Velaoras, D., Diamantopoulou, A., Sampatakaki, A., and Lykousis, V., 2016, Holocene climatic optimum centennial-scale paleoceanography in the NE Aegean (Mediterranean Sea). Geo-Mar. Lett. 36, 51-66.

Triantaphyllou, M.V., Ziveri, P., Gogou, A., Marino, G., Lykousis, V., Bouloubassi, I., Emeis, K.-C., Kouli, K., Dimiza, M., Rosell-Melé, A., Papanikolaou, M., Katsouras, G., and Nunez, N., 2009b, Late Glacial–Holocene climate variability at the south-eastern margin of the Aegean Sea: Marine Geology, v. 266, p. 182-197.

Triantaphyllou, M.V., Ziveri, P., and Tselepides, A., 2004, Coccolithophore export production and response to seasonal surface water variability in the oligotrophic Cretan Sea (NE Mediterranean). Micropaleontology 50, 127-144.

Velaoras, D., and Lascaratos, A., 2005, Deep water mass characteristics and interannual variability in the North and Central Aegean Sea. J. Mar. Syst. 53, 59-85.

Vergnaud-Grazzini, C., 1985, Mediterranean Late Cenozoic stable isotope record: stratigraphic and paleoclimatic implications. In: Stanley, D.J., Wezel, F.C. (Eds.), Geological Evolution of the Mediterranean Basin. Springer-Verlag, New York, pp. 413-451.

Vieira, L.E.A., Solanki, S.K., Krivova, N.A., and Usoskin, I., 2011, Evolution of the solar irradiance during the Holocene. Astron. Astrophys. 531, A6. .

Vink, A., Zonneveld, K.A.F., and Willems, H., 2000, Distributions of calcareous dinoflagellate cysts in surface sediments of the western equatorial Atlantic Ocean, and their potential use in palaeoceanography. Marine Micropaleontology 38, 149–180.

Volkman, J.K., Eglinton, G., Corner, E.D.S., and Forsberg, T.E.V., 1980, Long-chain alkenes and alkenones in the marine coccolithophorid Emiliania huxleyi. Phytochemistry 19, 2619-2622.

Waelbroeck, C., Mulitza, S., Spero, H., Dokken, T., Kiefer, T., and Cortijo, E., 2005, A global compilation of late Holocene planktonic foraminiferal δ18O: relationship between surface water temperature and δ18O: Quaternary Science Reviews, v. 24, p. 853-868.

Wanner, H., Beer, J., Bütikofer, J., Crowley, T.J., Cubasch, U., Flückiger, J., Goosse, H., Grosjean, M., Joos, F., Kaplan, J.O., Küttel, M., Müller, S.A., Prentice, I.C., Solomina, O., Stocker, T.F., Tarasov, P., Wagner, M., and Widmann, M., 2008, Mid- to Late Holocene climate change: an overview: Quaternary Science Reviews, v. 27, p. 1791-1828.

Wefer G., Berger W.H., Bijma J., and G., F., 1999, Clues to ocean history: A brief overview of proxies, in: G. Fischer, G. Wefer (Eds.), Use of Proxies in Paleoceanography: Examples from the South Atlantic, Springer, Berlin, pp. 1-68.

Xoplaki, E., 2002, Climate variability over the Mediterranean. PhD Thesis, University of Bern, Switzerland. Available through: http://sinus.unibe.ch/klimet/docs/phd_xoplaki.pdf.

Xoplaki, E., Fleitmann, D., Luterbacher, J., Wagner, S., Haldon, J.F., Zorita, E., Telelis, I., Toreti, A., and Izdebski, A., 2015, The Medieval Climate Anomaly and Byzantium : A review of the evidence on climatic fluctuations , economic performance and societal change: Quaternary Science Reviews, p. 1-24 http://dx.doi.org/10.1016/j.quascirev.2015.10.004.

Xoplaki, E., Gonzalez-Rouco, J.F., Gyalistras, D., Luterbacher, J., Rickli, R., and Wanner, H., 2003a, Interannual summer air temperature variability over Greece and its connection to the large scale atmospheric circulation and Mediterranean SSTs 1950-1999. Clim. Dyn. 20, 537-554.

Zervakis, V., Georgopoulos, D., and Drakopoulos, P., 2000, The role of the North Aegean in triggering the recent Eastern Mediterranean climatic changes. : J Geophys Res 105:26103–26116.